2 Excitation of Quadrupolar Nuclei in Solids

The quadrupole interaction causes a first-order frequency shift for satellite transitions and increases the spectral width of powder spectra. Short and powerful RF pulses are used to excite the spin system. High-power probes with a low quality factor $Q = \nu_c/\delta\nu_{\mathrm{probe}}$ during transmission are used, since a high quality factor and correspondingly small-bandwidth $\delta\nu_{\mathrm{probe}}$ would broaden a short RF pulse with the carrier frequency ν_c. Nevertheless, the width of the NMR spectrum is often equal to or broader than the spectral width of the RF pulse. Hence, the quadrupole interaction has to be considered for the Hamiltonian describing the interaction during the irradiation of the pulse. The theoretical expressions become more complicated, and the visualization of the effect of the pulse as a flipping of the magnetization vector no longer holds.

We introduce

$$\mathcal{H}^{\mathrm{size}} = \sqrt{\mathrm{Tr}\,\{\mathcal{H}^2\}} \tag{2.01}$$

as the magnitude of an observable related to the Hamiltonian. Divided by Planck's constant, it can be expressed as a frequency or a frequency interval. We assume the following relation:

$$\mathcal{H}_{\mathrm{L}}^{\mathrm{size}} \gg \mathcal{H}_{\mathrm{Q}}^{\mathrm{size}} \gg \mathcal{H}_{\mathrm{D}}^{\mathrm{size}}, \mathcal{H}_{\mathrm{CSA}}^{\mathrm{size}}. \tag{2.02}$$

The strength of the applied RF field, $\mathcal{H}_{\mathrm{RF}}^{\mathrm{size}}$, or nutation frequency, ν_{RF} (see Eq. (1.07)), and accordingly the interaction of the spins with the irradiated RF field, is variable. Experimentally, $\mathcal{H}_{\mathrm{RF}}^{\mathrm{size}}$ can be made to be large compared to $\mathcal{H}_{\mathrm{D}}^{\mathrm{size}}, \mathcal{H}_{\mathrm{CSA}}^{\mathrm{size}}$. However, the quadrupole interaction may easily exceed the maximum $\mathcal{H}_{\mathrm{RF}}^{\mathrm{size}}$. Thus, the strength of a quadrupole coupling, $\mathcal{H}_{\mathrm{Q}}^{\mathrm{size}}$in relation to $\mathcal{H}_{\mathrm{RF}}^{\mathrm{size}}$ has to be considered.

Continuous wave excitation is simpler to use in stationary experiments, as in the first decades of NMR, than in today's pulse experiments. Although one irradiates an extremely monochromatic wave in a stationary experiment, the excitation can be considered nonselective, since the system remains in thermal equilibrium, if sufficiently weak amplitudes of irradiation do not change the spin populations. When using pulse methods, the time the system requires to regain thermal equilibrium is long compared with the duration of the pulses. The amplitude of the RF pulses ensures that the population numbers are changed considerably and one faces a non-equilibrium situation; see [1] p. 40.

Below, we split the discussion of excitation by a single pulse or pulse train with a fixed carrier frequency into the following parts: spectral density of pulses, resonance offset, nonselective excitation, selective excitation of the central transition only, and partly selective excitation. Two sections are devoted to nutation and the two-pulse excitation of an FID. Then follow a discussion of excitation by cross polarization, a section about adiabatic passage and excitation by modulated pulsing, and finally, a section about excitation of very broad signals.

2.1 Spectral Density of Rectangular Pulses

A single rectangular pulse with the carrier frequency ω_c and the duration τ produces a frequency spectrum around ω_c that can be described by means of a cosine Fourier transform. The envelope of the RF spectrum has the form

$$f(\omega-\omega_c)=\int_{-\tau/2}^{+\tau/2}\cos[(\omega-\omega_c)t]\,\mathrm{d}t=\tau\frac{\sin[(\omega-\omega_c)\tau/2]}{(\omega-\omega_c)\tau/2}\,. \tag{2.03}$$

The function $f(\omega-\omega_c)$ equals τ for $\omega=\omega_c$ and is zero for integer values of the argument $(\omega-\omega_c)\tau/2\pi$. The first node in the frequency spectrum occurs at $\omega-\omega_c=2\pi/\tau$, in Hertz units at $\nu-\nu_c=1/\tau$. The spectral energy density, $E(\omega-\omega_c)=f^2(\omega-\omega_c)$, is proportional to the square of the RF field strength and can be normalized by

$$\int_{-\infty}^{+\infty}E(\omega-\omega_c)\,\mathrm{d}(\omega-\omega_c)=\frac{B_{RF}^2}{\mu_0}=\frac{\omega_{RF}^2}{\mu_0\gamma^2}\,. \tag{2.04}$$

This gives

$$E(\omega-\omega_c)=\frac{\omega_{RF}^2\,\tau}{2\pi\,\mu_0\gamma^2}\left[\frac{\sin[(\omega-\omega_c)\tau/2]}{(\omega-\omega_c)\tau/2}\right]^2\,. \tag{2.05}$$

The function in the square bracket equals 1 for $\omega\approx\omega_{c_0}$, and the spectral component of the energy density close to the carrier frequency of the pulse increases linearly with the pulse duration. Based on Eq. (2.05), we define the usable bandwidth of excitation, $\delta\omega_{bw}$, for a single rectangular pulse as

$$E\left(\omega-\omega_c=\pm\frac{1}{2}\delta\omega_{bw}\right)=\frac{1}{2}E(\omega=\omega_c)\,. \tag{2.06}$$

For $(\omega-\omega_c)\tau/2=1.3917$ we have $\left[\frac{\sin[(\omega-\omega_c)\tau/2]}{(\omega-\omega_c)\tau/2}\right]^2\approx 0.49992\approx\frac{1}{2}$. Therefore, the bandwidth of excitation by a single rectangular pulse width is in Hertz roughly equal to the reciprocal duration τ, or more accurately

$$\delta\nu_{bw}\approx\frac{0.886}{\tau}. \tag{2.07}$$

Pulse sequences consist of several pulses. We consider a train of odd numbers $(2n+1)$ of rectangular pulses with pulse distance T and extend Eq. (2.03) to

$$f(\omega-\omega_c)=\tau\frac{\sin[(\omega-\omega_c)\tau/2]}{(\omega-\omega_c)\tau/2}\left(1+2\sum_{k=1}^{n}\cos[k(\omega-\omega_c)T]\right). \tag{2.08}$$

The stimulated echo and the NOESY pulse sequences consist of three π/2 pulses. Figure 2.1 shows, as an example, the frequency spectrum of three 1-µs pulses with 10-µs distances in addition to the spectrum of a single rectangular 1-µs pulse.

However, a uniform excitation over a selected frequency range (rectangular excitation) is desired for many applications in NMR and MRI. For this purpose, the symmetric properties of the Fourier transform can be considered. A hypothetical pulse with the amplitude function $(\sin(bt))/t$ and an infinite duration $-\infty<t<\infty$ results in a cosine Fourier transform with a rectangular shape and a bandwidth of $\delta\nu_{bw}=b/\pi$ around the carrier frequency ν_c. But finite pulses should be used for

practical reasons, and the complex character of the Fourier transform has to be considered. Kupče and Freeman [2] considered HS pulses with a hyperbolic secant function of time (see Ref. [3] p. 99 and Ref. [4]) and introduced WURST pulses (wide-band, uniform rate, smooth truncation) with a characteristic sausage shape. HS and WURST pulses are finite and consist of real and imaginary components. HS pulses are analogous to the $(\sin(bt))/t$ function; see Fig. 3 in [2].

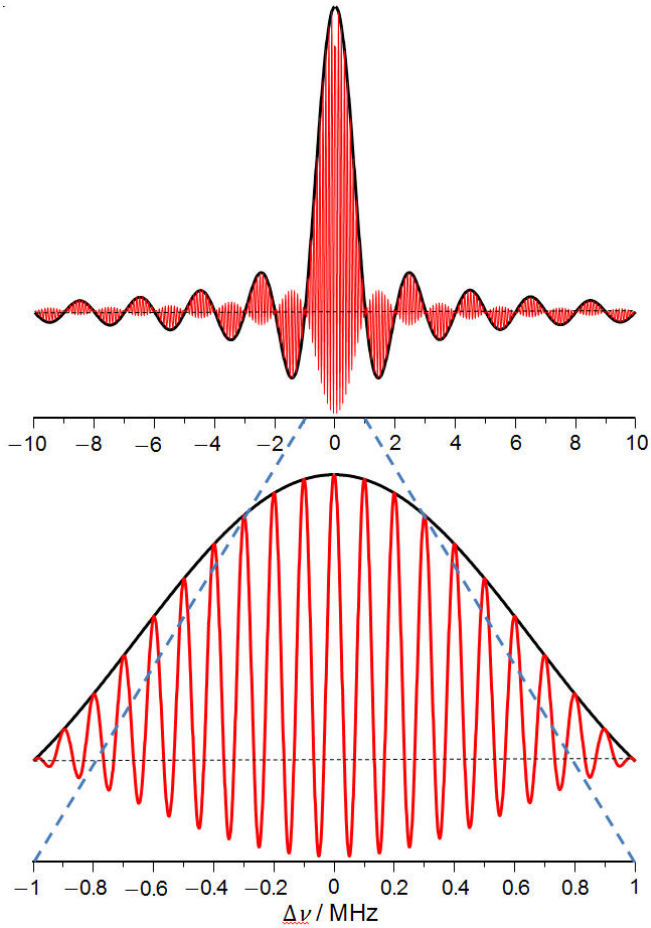

Fig. 2.1. Spectral densities of a pulse with 1-µs pulse duration (bold lines) and a pulse train consisting of 3 pulses with 1-µs pulse duration and pulse distances of 10 µs (narrow lines). The lower picture shows the range between the first zero crossings for the single pulse.

A chirp denotes in electronic engineering a signal with a time-dependent carrier frequency. It is well-known in electronics that phase modulation has the same effect as frequency modulation. Chirped pulses do not overcome the basic problem of the limited bandwidth of excitation, but they provide a nearly uniform excitation over the limited spectral range of the pulse and are popular now in many areas of NMR [5]. For example, Bhattacharyya and Frydman [6] demonstrated that the observation of a 80-kHz broad ^{35}Cl NMR signal of polycrystalline ornithine hydrochloride by the Fourier transform of an echo after two chirped pulses (modified WURST pulses [2]) is superior to two rectangular pulses with respect to the signal-to-noise ratio and the distortions of the echo after non-uniform excitation. O'Dell [7] presented a WURST review in 2013.

2.2 Resonance Offset

Description of the FID (see Section 1.4) is accomplished by choosing the carrier frequency, ω_c, of the pulse for the transformation into the interaction representation (see Section 1.3). The difference between the resonance frequency of the nuclear spin, ω_L, and the carrier frequency, ω_c, of an applied RF pulse is called the *resonance offset*. For the detection of the NMR signal, in the absence of pulsing, the same frequency ω_c with a tunable phase is used for the demodulation of the signal. Therefore, the effect of a resonance offset is in the case of *detection* simply the result of the

difference between the Larmor frequency and the reference frequency, which causes a frequency shift of the signal in the Fourier transform spectrum.

For the *excitation,* however, a resonance offset causes the mean of the excitation spectral density to be shifted with respect to the resonance frequency of the spin. Between pulses, the phase of the magnetization in the x,y-plane changes with time as the result of the offset; thus, the relative phase with respect to the next pulse becomes time dependent, as well.

For spin-1/2 nuclei and a negligible homogeneous interaction the influence of a resonance offset during pulsing is typically described using an *effective* magnetic RF field, B_{eff}, instead of B_{RF}.
We rewrite the operator $U_{\mathrm{i}}(t, t_0)$ in Eq. (1.23) by means of Eqs. (1.27) and (1.29) as

$$U_{\mathrm{i}}(t, t_0) = \exp\{-\mathrm{i}(\Delta\omega\, I_z + \omega_{\mathrm{RF}}\, I_y)(t - t_0)\} \tag{2.09}$$

and explain it by a rotation around the angle α in 3-dimensional space: Comparison with Eq. (1.10) using the rotation angle α instead of Ω gives

$$n_y\alpha = -\omega_{\mathrm{RF}}\,(t - t_0), \text{ and } n_z\alpha = -\Delta\omega\,(t - t_0). \tag{2.10}$$

From the normalization of the axis of rotation, $\boldsymbol{n}$, we have

$$1 = \boldsymbol{n}^2 = \left(\omega_{\mathrm{RF}}^2 + \Delta\omega^2\right)\frac{t - t_0}{\alpha^2} \tag{2.11}$$

and

$$|\alpha| = |t - t_0|\sqrt{\omega_{\mathrm{RF}}^2 + \Delta\omega^2}. \tag{2.12}$$

The angle between the axis of rotation, $\boldsymbol{n}$, and the laboratory z-axis is

$$\alpha = -\arcsin\frac{\omega_{\mathrm{RF}}}{\sqrt{\omega_{\mathrm{RF}}^2 + \Delta\omega^2}.} \tag{2.13}$$

For the effective angular frequency, $\omega_{\mathrm{RF}}^{\mathrm{eff}}$, of this rotation about the axis $\boldsymbol{n}$, we get

$$\omega_{\mathrm{RF}}^{\mathrm{eff}} = \sqrt{\omega_{\mathrm{RF}}^2 + \Delta\omega^2}. \tag{2.14}$$

With the gyromagnetic ratio γ, this leads to a definition of the effective magnetic RF field:

$$B_{\mathrm{RF}}^{\mathrm{eff}} = \omega_{\mathrm{RF}}^{\mathrm{eff}}/\gamma. \tag{2.15}$$

The resonance offset during pulsing causes the magnetization to rotate about an effective magnetic field, $B_{\mathrm{RF}}^{\mathrm{eff}}$, which is inclined at angle α in relation to the laboratory z-axis. Without offset, i.e., $\Delta\omega = 0$, we have $\alpha = 90°$.

The picture of the effective magnetic RF field can also be applied if the resonance line is inhomogeneously broadened: however, for quadrupole broadened lines it fails, since the frequency components of the NMR signal belong to different transitions in the spin system. Only if each transition of a single crystal could be excited separately would it be possible to define the effective magnetic RF fields for a single transition. However, for the more interesting case of partly selective excitation, spin-flipping during pulsing in one transition is closely related to the spin-flipping in another transition, so that the influence of the resonance offset during or between pulsing cannot be simplified.

2.3 Nonselective Excitation

Nonselective excitation is defined by two restrictions. First, the pulse has to be strong compared with the internal interactions,

$$\mathcal{H}_{\mathrm{RF}}^{\mathrm{size}} \gg \mathcal{H}_{\mathrm{Q}}^{\mathrm{size}}, \mathcal{H}_{\mathrm{D}}^{\mathrm{size}}, \mathcal{H}_{\mathrm{CSA}}^{\mathrm{size}}, \tag{2.16}$$

in order to predominantly drive the evolution of the spin system by the interaction with the irradiated RF field. In this case the pulse is called a *hard* pulse. Second, the bandwidth of the probe circuit, $\delta\nu_{\mathrm{probe}}$, and the bandwidth of excitation pulse, $\delta\nu_{\mathrm{bw}}$, have to meet

$$\delta\nu_{\mathrm{probe}} = \frac{\nu_{\mathrm{c}}}{Q}, \delta\nu_{\mathrm{bw}} \gg \frac{1}{h}\mathcal{H}_{\mathrm{Q}}^{\mathrm{size}}, \frac{1}{h}\mathcal{H}_{\mathrm{D}}^{\mathrm{size}}, \frac{1}{h}\mathcal{H}_{\mathrm{CSA}}^{\mathrm{size}}. \tag{2.17}$$

Here, a zero-offset of the carrier frequency, ν_{c}, with respect to the Larmor frequency, ν_{L}, is supposed; Q stands for the quality factor of the probe during transmission and h for Planck's constant. Internal interactions within the spin system can be neglected during pulsing, if Eqs. (2.16) and (2.17) are fulfilled. This means that lowering the quality factor for transmission increases the bandwidth. Unfortunately, lowering the quality factor during detection decreases the sensitivity of the probe circuit. Quality factors for transmission (excitation) and detection are different but cannot be optimized independently.

A pulse is called *partly selective* or *selective* if Eq. (2.17) does not hold. The pulse is termed *soft* if it does not satisfy Eq. (2.16).

For nonselective excitation we can neglect the influence of the quadrupole coupling during the action of an RF pulse. Therefore, the Hamiltonian in the interaction representation of the effect of a single y-pulse is time-independent, $\mathcal{H}_{\mathrm{RF,i}} = \hbar\omega_{\mathrm{RF}} I_y$ (see Eq. (1.29)), and we can neglect the Zeeman term of Eq. (2.09) in the evolution operator:

$$U_{\mathrm{i}}(t, t_0) = \exp\{-\mathrm{i}\,\omega_{\mathrm{RF}}\, I_y\,(t - t_0)\}. \tag{2.18}$$

If the spin system is in the thermal equilibrium before the pulse starts, at $t_0 = -\tau$, the corresponding density operator is $|\rho_0\rangle = |I_z\rangle$; see Eq. (1.32). After a pulse with the duration τ, one obtains, for $t = 0$,

$$|\rho_{\mathrm{i}}(\tau)\rangle == \exp\{-\mathrm{i}\,\omega_{\mathrm{RF}}\, I_y\,\tau\}|I_z\rangle = \cos(\omega_{\mathrm{RF}}\,\tau)|I_z\rangle + \sin(\omega_{\mathrm{RF}}\,\tau)|I_x\rangle. \tag{2.19}$$

For the intensity of the FID, $G(t = 0)$, it is inferred from Eq. (1.33) that

$$G(0) = \frac{\langle I_-|\rho_{\mathrm{i}}(t)\rangle}{\langle I_x|I_x\rangle} = \sin(\omega_{\mathrm{RF}}\,\tau). \tag{2.20}$$

After the pulse, $t \geq 0$, the quadrupole interaction is assumed to govern the evolution of the density operator. If in the interaction representation the truncated quadrupole coupling, $\mathcal{H}_{\mathrm{Q}}^{(0)}$, is used (Eq. (1.61)), the evolution operator $U_{\mathrm{i}}(t, t_0)$ is obtained by integrating Eq. (1.22) with Eq. (1.61):

$$U_{\mathrm{i}}(t, t_0) = \exp\left\{-\mathrm{i}\frac{\omega'_{\mathrm{Q}}}{6}[3I_z^2 - I(I+1)]t\right\}. \tag{2.21}$$

Based on Eq. (2.21) and Eq. (2.19), $G(t)$ is given by

$$G(t) = \frac{1}{\langle I_x|I_x\rangle} = \sum_{m=-1}^{I-1} 2W_m \langle m|\rho_{\mathrm{i}}(t)|m+1\rangle \exp\{-\mathrm{i}\omega'_{\mathrm{Q}}(m+1/2)t\}, \tag{2.22}$$

where the trace is taken in the I_Z representation, and

$$W_m = \tfrac{1}{2}\sqrt{I(I+1) - m(m+1)} = \tfrac{1}{2}\sqrt{(I-m)(I+m+1)}. \tag{2.23}$$

$2I$ quadrupole transitions cause $2I$ components of the FID, given by Eq. (2.22), with amplitudes given by Eq. (2.21). For the central transition, $m = -1/2$, the time-dependence in Eq. (2.22) vanishes:

$$G_{-1/2,1/2}(0) = \frac{2W_{-1/2}^2}{\langle I_x|I_x\rangle}\sin(\omega_{\mathrm{RF}}\,\tau) = \frac{3(2I+1)}{8I(I+1)}\sin(\omega_{\mathrm{RF}}\,\tau), \tag{2.24}$$

where $\langle I_x|I_x\rangle = tr\,\{I_x^2\} = \frac{1}{3}I(I+1)(2I+1)$. Generally, the intensity of any transition, $m \to m+1$, is given by

$$G_{m,m+1}(0) = \frac{3[I(I+1) - m(m+1)]}{2I(I+1)(2I+1)}\sin(\omega_{\mathrm{RF}}\,\tau) = f(I,m)\sin(\omega_{\mathrm{RF}}\,\tau). \tag{2.25}$$

For the nonselective excitation is the $(\omega_{\mathrm{RF}}\,\tau)$-dependent intensity of the FID, $G(0)$, sinusoidal for all quadrupole transitions, as for spin-1/2 nuclei. The factor $f(I,m)$ corresponds to the relative intensities of the transitions and is numerically presented in Table 2.1.

Table 2.1. $f(I,m)$ of Eq. (2.24) describing the relative intensities of the transitions $m \to m+1$ of half-integer spins I.

$I \mid m$	$-\frac{9}{2}$	$-\frac{7}{2}$	$-\frac{5}{2}$	$-\frac{3}{2}$	$-\frac{1}{2}$	$+\frac{1}{2}$	$+\frac{3}{2}$	$+\frac{5}{2}$	$+\frac{7}{2}$
$\frac{1}{2}$					1				
$\frac{3}{2}$				$\frac{3}{10}$	$\frac{4}{10}$	$\frac{3}{10}$			
$\frac{5}{2}$			$\frac{5}{35}$	$\frac{8}{35}$	$\frac{9}{35}$	$\frac{8}{35}$	$\frac{5}{35}$		
$\frac{7}{2}$		$\frac{7}{84}$	$\frac{12}{84}$	$\frac{15}{84}$	$\frac{16}{84}$	$\frac{15}{84}$	$\frac{12}{84}$	$\frac{7}{84}$	
$\frac{9}{2}$	$\frac{9}{165}$	$\frac{16}{165}$	$\frac{21}{165}$	$\frac{24}{165}$	$\frac{25}{165}$	$\frac{24}{165}$	$\frac{21}{165}$	$\frac{16}{165}$	$\frac{9}{165}$

Intensity measurements

For the determination of the concentration of the quadrupolar nuclei under study, the common conditions for all NMR intensity measurements must first be fulfilled:

(■) The reference sample, S_r, should contain the same nuclei with a similar line width of the NMR signal as the sample under study, S_x;
(■■) S_r and S_x should have the same sample shapes, for example powders in identical sample containers like MAS rotors, in order to avoid effects due to the $\boldsymbol{B}_{\mathrm{RF}}$ inhomogeneity; and
(■■■) The repetition time has to be longer than $5T_1$ for S_r and S_x.

Additional conditions for quadrupolar nuclei in the case of *nonselective* excitation:
(★) The excitation bandwidth of the pulse, $\delta\nu_{\mathrm{bw}}$, see Eq. (2.07), has to be larger than the spectrum width, Fig. 1.2; which is $2\nu_{\mathrm{Q}}$, $4\nu_{\mathrm{Q}}$ and $6\nu_{\mathrm{Q}}$ for $I = 3/2$, $I = 5/2$ and $I = 7/2$, respectively); and **(★★)** the band width of the probe $\delta\nu_{\mathrm{probe}}$ has to be larger than the spectrum width as well. Conditions **(★)** and **(★★)** give an upper limit for the quadrupole frequency $\nu_{\mathrm{Q}} \lesssim 1\ \mathrm{MHz}/(I + 1/2)$, since the maximum values for $\delta\nu_{\mathrm{bw}}$ and $\delta\nu_{\mathrm{probe}}$ are both about 1 MHz for a high-power amplifier and probe.

2.4 Selective Excitation of a Single Transition

For most non-cubic substances, a nonselective excitation is not achievable. In such cases the exciting pulse is called a *soft* pulse

$$\mathcal{H}_{\mathrm{RF}}^{\mathrm{size}} \lesssim \mathcal{H}_{\mathrm{Q}}^{\mathrm{size}}. \tag{2.26}$$

For a single crystal with sufficiently large quadrupole coupling, it is always possible to tune to each transition separately. But for powders, a selective pulse can only be applied to excite the central transition. Since the first-order quadrupole shift of the satellite signals depends on the orientation of the electric field gradients with respect to the static field, for crystallite powders or glassy materials part of the satellite signal always resides within the spectral range of the central transition. For a selective excitation of the central transition, the fraction of excited satellites should be sufficiently small. In principle this can be achieved, if by prolongation of the pulse length the bandwidth of excitation, $\delta\nu_{\mathrm{bw}}$, only slightly exceeds the spectral width of the central transition. But in the case of magic-angle spinning we have weak excitation of all transitions if the pulse duration becomes equal to or longer than the rotation period.

The excitation of a single transition can be treated as a fictitious spin-1/2 system [1] by choosing the appropriate 2-by-2 submatrix out of the corresponding $(2I+1)$-dimensional matrix and decomposing it into spin-1/2 matrices, S_x, S_y, S_z. For the submatrix out of I_Z with $\hat{1}$ as the unity operator, the $m \rightarrow m+1$ transition yields

$$\begin{pmatrix} m+1 & 0 \\ 0 & m \end{pmatrix} = \frac{2m+1}{2} \begin{pmatrix} 1 & 0 \\ 0 & 1 \end{pmatrix} + \begin{pmatrix} 1/2 & 0 \\ 0 & -1/2 \end{pmatrix} = \frac{2m+1}{2}\,\hat{1} + S_z\,. \tag{2.27}$$

For the submatrix , I_Z^2 , we get

$$\begin{pmatrix} (m+1)^2 & 0 \\ 0 & m^2 \end{pmatrix} = \frac{2m^2+2m+1}{2}\hat{1} + (2m+1)S_z, \tag{2.28}$$

and for the *y*-component, I_y,

$$\begin{pmatrix} 0 & -\mathrm{i}W_m \\ \mathrm{i}W_m & 0 \end{pmatrix} = \frac{W_m}{V_{-1/2}} \begin{pmatrix} 0 & -\mathrm{i}V_{-1/2} \\ \mathrm{i}V_{-1/2} & 0 \end{pmatrix} = 2W_m S_y, \tag{2.29}$$

where W_m is defined by Eq. (2.23), and $V_{-1/2} = W_{-1/2}^{I=1/2} = 1/2$.

The analog to Eq. (2.19) for selective excitation reads

$$|\rho_{\mathrm{i}}(\tau)\rangle == \exp\{-\mathrm{i}\,2W_m\omega_{\mathrm{RF}}\,S_y\,\tau\}|S_z\rangle = \frac{2m+1}{2}\,\hat{1} + \cos(2W_m\omega_{\mathrm{RF}}\,\tau)S_z\rangle + \sin(2W_m\omega_{\mathrm{RF}}\,\tau)|S_x\rangle. \tag{2.30}$$

Finally, for the intensity of the NMR signal of the $m \to m+1$ transition after a selective pulse with a flip angle $\omega_{\mathrm{RF}}\,\tau$, we get

$$G^{\mathrm{sel}}_{m,m+1}(0) = \frac{2W_m}{\langle I_x|I_x\rangle}\langle -1/2|\rho_{\mathrm{i}}(\tau)|1/2\rangle \sin(2W_m\,\omega_{\mathrm{RF}}\,\tau) = \frac{3W_m}{I(I+1)(2I+1)}\sin(2W_m\omega_{\mathrm{RF}}\,\tau), \quad (2.31)$$

because the contributions arising from the first and second term on the right-hand side of Eq. (2.30) vanish. Comparison with Eq. (2.25) reveals that the maximal observed intensity is reduced by $2W_m$, but the selective nutation frequency is enhanced, as

$$\omega^{\mathrm{sel}}_{\mathrm{RF}} = 2W_m\,\omega_{\mathrm{RF}}\,. \quad (2.32)$$

For the central transition, $m = -1/2$, we obtain from Eq. (2.31)

$$G^{\mathrm{sel}}_{-1/2,1/2}(0) = \frac{3}{4I(I+1)}\sin[(I+1/2)\,\omega_{\mathrm{RF}}\,\tau]. \quad (2.33)$$

The maximal observed intensity is reduced with respect to the nonselective excitation by $(I+1/2)$ and we have

$$\omega^{\mathrm{sel}}_{\mathrm{RF}} = (I+1/2)\,\omega_{\mathrm{RF}}\,. \quad (2.34)$$

Expressions like *solid* or *liquid* π-pulse for $\omega^{\mathrm{sel}}_{\mathrm{RF}} = \pi$ and $\omega_{\mathrm{RF}} = \pi$, respectively, will not be used in this review because they are often misused in the literature.

In the photon language, the understanding of nonselective and selective excitation is the following: The spin-flipping within $2I+1$ energy levels due to excitation corresponds to the absorption and stimulated emission of photons. The number of photons in the spectral range of excitation is proportional to the spectral energy density $E(\omega-\omega_{\mathrm{c}})$, Eq. (2.05). If the bandwidth of excitation, $\delta\omega_{\mathrm{bw}}$, is large compared to the spectral range of transitions for the spin system, the excitation is nonselective. After a π-pulse, the population difference is inverted, or, after a $\frac{\pi}{2}$-pulse, the population difference is zero. In the high-temperature approximation, the population number N_m of the Zeeman level E_m can be written as $N_m = 2m$. Then, e. g., for $I = \frac{5}{2}$, the population of the $2I+1 = 6$ level is $-5, -3, -1, 1, 3, 5$. The conservation of energy, together with the selection rule $\Delta m = \pm 1$, shows that after a $\frac{\pi}{2}$-pulse in each of the $2I = 5$ transitions, $m \to m+1$, the net number of absorbed photons is $5, (5+3), (5+3+1), (5+3), 5$ for $m = -\frac{5}{2}, -\frac{3}{2}, -\frac{1}{2}, \frac{1}{2}, \frac{3}{2}$, respectively. These are the relative intensities of the 5 transitions for nonselective excitation. For a selective excitation of the central transition, the net number of absorptions after a $\pi/2$-pulse is 1, as for any other single transition. In order to compare the number of absorptions with those for nonselective excitation, we have to recall that the observed intensity is proportional to the number of absorbed photons per unit time and proportional to the number of incident photons with the appropriate frequency [8]. Suppose ω_{RF} remains constant; then the difference in time for reaching zero population difference for selective and nonselective excitation can be deduced from Eq. (2.05). Since the number of incident photons, $E(\Omega=0) \sim \tau$, increases with time and the total number of absorptions is quadratic in τ, we find for the pulse durations τ_{ns} and τ_{sel}, which are necessary to cancel the population differences for nonselective and selective excitation, respectively, the ratio $(\tau_{\mathrm{ns}}/\tau_{\mathrm{sel}})^2 = 9/1$ for $I = 5/2$. If τ remained constant for both kinds of excitations and ω_{RF} was changed in order to reach the zero-population difference, one would get the same result since $E(\omega-\omega_{\mathrm{c}}) \sim \omega^2_{\mathrm{RF}}$. Thus, for comparison of the maximum intensities for the central transitions, for both nonselective and selective excitation, $I^{\max}_{\mathrm{ns}}$ and $I^{\max}_{\mathrm{sel}}$, one finds in accordance with Eqs. (2.24) and (2.31) for $I = 5/2$ that $I^{\max}_{\mathrm{ns}}/I^{\max}_{\mathrm{sel}} = 9\;\tau_{\mathrm{sel}}/\tau_{\mathrm{ns}} = 3$.

Intensity measurements
Additional conditions for the determination of the concentration of the quadrupolar nuclei under study are different in the case of *selective excitation of the central transition* compared to the *nonselective excitation of all transitions*. The common conditions for intensity measurements are given at the end of Section 2.3. Additional conditions can be derived from Fig. 1.3 and are mostly fulfilled in the case of *selective* excitation. They are:

(★) the maximum width of the central transition spectrum is $(\nu_{\mathrm{Q}}^2/3\nu_{\mathrm{L}})[I(I+1)-3/4]$ for $\eta = 1$ and has to be smaller than the excitation bandwidth of the pulse, $\delta\nu_{\mathrm{bw}}$ (see Eq. (2.07)), and
(★★) it has to be smaller than the band width of the probe $\delta\nu_{\mathrm{probe}}$ as well.
A minor problem arises because a pure selective excitation of the central transition cannot be achieved for powder samples; see Section 2.5.

Comparing Eqs. (2.33) and (2.24), it can be seen that the maximum intensity of the central transition for the optimum flip angle decreases by $1/(I+1/2)$ going from nonselective to selective excitation. However, for small flip angles we have $\sin[(I+1/2)\,\omega_{\mathrm{RF}}\,\tau] \approx (I+1/2)\,\omega_{\mathrm{RF}}\,\tau$, and the two intensities in Eqs. (2.33) and (2.24) are approximately equal. For any spin and any ratio $\omega_{\mathrm{Q}}/\omega_{\mathrm{RF}}$ we obtain a relative intensity deviation of less than 10% using a reduced flip angle [9]

$$\omega_{\mathrm{RF}}\,\tau \leq \frac{\pi}{4(I+1/2)}. \tag{2.35}$$

As long as Eq. (2.35) is fulfilled, the observed NMR intensity does not depend on the quadrupole interaction, and the measured intensities can be compared directly. However, it should be emphasized that the dependencies given by Eqs. (2.33) and (2.24) describe the intensities of the central transition. The contributions from the satellites within the spectral range of the central transition are neglected. Therefore, we emphasize the condition **(■)** noted at the end of Section 2.3 that the sample under study and the reference sample should have similar line widths, indicating a similar quadrupole broadening of the NMR signal.

2.5 Partly Selective Excitation of More Than One Transition

As mentioned above, a pure selective excitation of the central transition cannot be achieved for powder samples. Some nuclei are impacted by an electric field gradient tensor with an angle between the z-axis and the external magnetic field that is near to the magic angle. For these nuclei we obtain ω'_{Q} in Eq. (1.58) ≈ 0. Thus, some satellite transitions will occur even if selective excitation is achieved. If the spectral width of the central transition is small compared with ω_{RF} and second-order quadrupole effects can be neglected, we have to analyze the equation

$$|\rho_{\mathrm{i}}(\tau)\rangle \;== \exp\left\{-\mathrm{i}\left[\,\omega_{\mathrm{RF}}\,I_y \;+\frac{1}{6}\,\omega'_{\mathrm{Q}}(3I_z^2 + I(I+1))\right]\tau\right\}|I_z\rangle, \tag{2.36}$$

in which the influence of the first-order quadrupole Hamiltonian during the pulse is considered. Since an analytical solution of Eq. (2.36) is rather complicated, numerical calculations were used to define the dependence of the intensity of the central line on $\omega_{\mathrm{RF}}\tau$ using the parameter $r = \omega'_{\mathrm{Q}}/\omega_{\mathrm{RF}}$ [9, 10]. It results in sine functions with the period $\omega_{\mathrm{RF}}\tau = 2\pi$ for $r = 0$ and, e. g. for $I = 5/2$, periods $\omega_{\mathrm{RF}}\tau = 2\pi/2$ for $r \approx 3.12$ and $2\pi/3$ for $r = \infty$ [9]. But the functions become non-sinusoidal if the *powder averages* are calculated for values other than $r = 0, \infty$; see Fig. 2.2.

Nielsen *et al.* [11] considered the excitation of $I = 3/2$ and $I = 5/2$ nuclei in the case of magic-angle spinning. Since under MAS the orientation-dependent EFG is averaged over the duration of the pulse, the quadrupole interaction appears to be smaller, depending on spinning speed and pulse duration.

The majority of solid-state NMR experiments on half-integer spin quadrupolar nuclei are performed under MAS conditions. But we did not consider the sample rotation for the excitation, since the pulse length, except for nutation experiments, is usually much shorter than the rotation period.

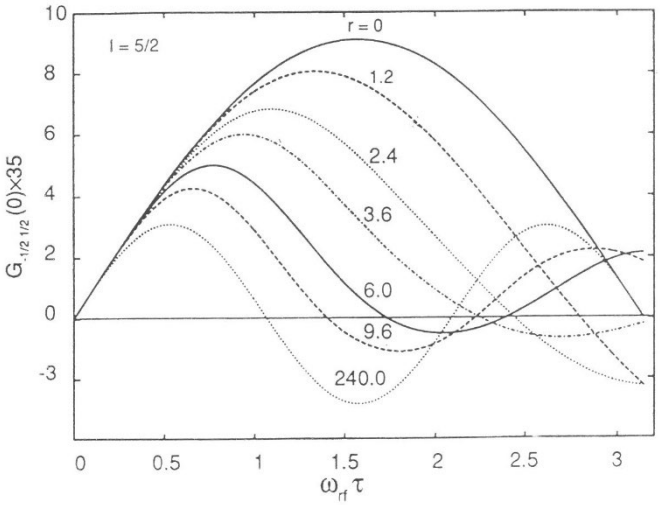

Fig. 2.2. Results for the powder average of the dependence of the central line intensity on the flip angle for I = 5/2. The curves show the strongest deviation from sinusoidal behavior for $r \approx 3.6$. The figure was taken from Ref. [12].

2.6 Nutation Techniques

The original NMR nutation experiment by Torrey [13] in 1949 showed the nutation of the resultant nuclear magnetic moment vector by applying radio frequency pulses with a carrier frequency close to the resonance frequency of the spins. From 1983 to 2001 about 80 solid-state NMR studies were dedicated to half-integer quadrupolar nuclei following the work of Samoson and Lippmaa [14, 15], who introduced two-dimensional nutation NMR.

The simple 2D experiment is divided into the evolution period t_1, during which a strong RF field is irradiated, and a detection period t_2 for the observation of the FID. In the rotating frame, the spins *nutate* (precess) around the strong RF field with specific nutation frequencies ω_1. Here the subscript 1 denotes the frequency axis ω_1 in the 2D-spectrum corresponding to the Fourier transform with respect to t_1 and should not be confused with $\omega_{\mathrm{RF}} = -\gamma B_{\mathrm{RF}}$ which is a constant for the 2D experiment. For quadrupolar nuclei the nutation frequencies ω_1 depend on the strength of the quadrupole interaction. If $\omega_{\mathrm{Q}} \ll \omega_{\mathrm{RF}}$, then the transverse magnetization responds to the RF pulse like spin-1/2 nuclei; thus, $\omega_1 = \omega_{\mathrm{RF}}$. If $\omega_{\mathrm{Q}} \gg 10\ \omega_{\mathrm{RF}}$, the central transition can be treated as a two-level system and one nutation frequency is expected, but this frequency is increased by a factor $(I + 1/2)$; i. e. $\omega_1 = (I + 1/2)\ \omega_{\mathrm{RF}}$ (see Eq. (2.34)). For the intermediate case in the range $1 < \omega_{\mathrm{Q}} / \omega_{\mathrm{RF}} < 100$, the nutation spectra reflect the influence of the partly excited outer transitions. The ratio $r = \omega_{\mathrm{Q}} / \omega_{\mathrm{RF}}$ is varied as the parameter for the acquisition of the nutation spectra.

NMR nutation spectroscopy of quadrupolar nuclei has been reviewed in the past [12, 16, 17] and in 2012 by Kentgens [18]. The NMR nutation technique was substituted by other NMR techniques at the beginning of the current century. Mostly in NQR is the nutation spectroscopy of quadrupolar nuclei still in use [19]. Recent studies of Kentgens and coworkers [20, 21] used a nutation NMR experiment SATURN (SAtellite Transition nUtation of quadRupolar Nuclei) to discriminate central and satellite transitions. The experiment allows the assignment of central and satellite transitions in the case of distributions in quadrupole parameters.

2.7 Two-pulse Free Induction Decay

The two-pulse free induction decay monitors the quadrupole interaction similar to the nutation technique. The information of the first-order quadrupole interaction is transformed onto the central transition intensity by two pulses [12] as first reported in Ref. [22]. At the beginning, the quadrupole nucleus is excited by a hard y-pulse with $\omega_{\mathrm{RF}}\,\tau \ll 1$. Then, immediately after the pulse there appear $2I$ components of magnetization, polarized in the x-direction. These $2I$ components have a resonance offset $\Delta\omega$ in the rotating frame due to the first-order quadrupole interaction: $\Delta\omega_m = (2m+1)\omega'_{\mathrm{Q}}$, where m runs from $-I, -I+1, \ldots, I-1$, see Eq. (2.22). The x-components of these polarizations vary with $\cos\left[(2m+1)\omega'_{\mathrm{Q}}t\right]$. A second hard y-pulse at time $t = t_1$ creates a new x-component formed by spins that are still in the z-direction after the first pulse. Then, with respect to the polarizations created by the first pulse, it affects only spins polarized in the x-direction, the number of which is proportional to $\cos\left[(2m+1)\omega'_{\mathrm{Q}}t_1\right]$, at the time $t = t_1$. Hence, depending on the time delay between the pulses, a varying number of spins forming the satellite transitions will be transferred into the central transition. Since these contributions are sinusoidal in $\omega'_{\mathrm{Q}}t_1$ the intensity of the central transition is modulated by $\cos\left[(2m+1)\omega'_{\mathrm{Q}}t_1\right]$. A second Fourier transform of the dependence of the intensity of the central transition on the pulse length t_1 should give definite contributions at frequencies $\omega_m = (2m+1)\omega'_{\mathrm{Q}}$.

A theoretical analysis of this effect has been reported [22, 23] for the case of nonselective pulses, the phase shifting between pulses has been discussed, and information about the quadrupole parameter of ^{27}Al in powdered alum, corundum, and low-cristobalite has been obtained. Man [24, 25] described the experiment for $I = 3/2$ with the fictitious spin-$1/2$ operator formalism using two in-phase RF pulses with a short delay between them and variable length of the second pulse, and in addition, with an alternating pulse phase and alternating receiver phase [26]. The quadrupole coupling of ^{23}Na in powdered $NaNO_3$ [25] and of ^{7}Li in a single crystal of $LiTaO_3$ [24, 26] were studied by the dependence of the central line intensity on the width of the second RF pulse. Man performed several studies by means of this technique, calling them *two-pulse nutation experiments*; see http://www.pascal-man.com/presentation/two-pulses.shtml#-1. However, the term *nutation* is misleading here, since the development takes place between the pulses in the absence of RF irradiation. The last study was devoted to ^{51}V nuclei in a single ferroelastic crystal of $BiVO_4$ [27]. It should be noted that the t_1 increment has to be one rotation period, or a multiple of it, if MAS is also to be applied.

2.8 Cross Polarization

Cross polarization (CP) was introduced as an excitation technique by Hartmann and Hahn [28] and was applied to the proton-enhanced NMR of dilute spins in solids by Pines, Gibby and Waugh [29]. A detailed discussion of CP experiments can be found in the textbook by Slichter [30], pp. 277. CP of half-integer quadrupolar nuclei was first applied by S. Vega [31] to single crystals and is discussed in his review [32].

The combination of CP with MAS is now widely used for the polarization transfer in solid-state NMR, mainly from ^{1}H to low-sensitivity spin-1/2-nuclei, and provides increased sensitivity for the MAS spectra of the low-sensitivity spin-1/2-nuclei, which mostly have a longer longitudinal relaxation time than ^{1}H nuclei. Its application to quadrupolar nuclei with half-integer spins is now established as well. It is more used for spectral editing than for enhancement of sensitivity, since the T_1 of quadrupolar nuclei is typically shorter than that for ^{1}H nuclei. About 200 ^{27}Al[^{1}H] CP MAS NMR studies were published after the first paper by Blackwell and Patton [33]; other quadrupolar nuclei with half-integer spins were also excited by CP. Heteronuclear correlation (HETCOR) studies using CP for mixing between ^{27}Al and ^{31}P nuclei in both directions were introduced by Fyfe *et al.* [34].

Beginning with the study of Pruski *et al.* [35], CP has been used for spectral editing of multiple-quantum (MQ) MAS NMR spectra in many studies. The polarization transfer is performed from ^{1}H, ^{19}F or ^{31}P nuclei and limited to the central transition of the quadrupolar nucleus, Q, with spin I in the majority of studies and the opposite direction in a few. The mixing pulse for CP is relatively long and accordingly has a relatively narrow bandwidth. In this case, the Hartmann-Hahn condition [28] requires equality between the nutation frequencies of the ^{1}H nuclei, $\omega_{\mathrm{RF}}^{\mathrm{H}}$, and of the quadrupolar nuclei for selective excitation, $\omega_{\mathrm{RF}}^{\mathrm{Q\,sel}}$ (see Eq. (2.34)):

$$\omega_{\mathrm{RF}}^{\mathrm{Q\,sel}} = (I + 1/2)\,\omega_{\mathrm{RF}}^{\mathrm{Q}} = -(I + 1/2)\,\gamma_{\mathrm{Q}} B_{\mathrm{RF}}^{\mathrm{Q}} = -\gamma_{\mathrm{H}} B_{\mathrm{RF}}^{\mathrm{H}} = \omega_{\mathrm{RF}}^{\mathrm{H}}. \tag{2.37}$$

A.J. Vega [36, 37] considered the spin dependence of CP MAS NMR of spin-3/2 nuclei on the ratio $\alpha = \nu_{\mathrm{RF}}^2/\nu_{\mathrm{Q}}\nu_{\mathrm{rot}}$. He found a greatly reduced spin-lock efficiency for the intermediate case $\alpha = 4$ and more efficient polarization transfer for $\alpha \gg 1$ and $\alpha \ll 1$. However, an upper limit of α is given by the overlap of sidebands for slow spinning speeds. In the limit of fast spinning, the Hartmann-Hahn matching must satisfy a sideband condition,

$$\nu_{\mathrm{RF}}^{\mathrm{H}} = (I + 1/2)\,\nu_{\mathrm{RF}}^{\mathrm{Q}} \pm n\,\nu_{\mathrm{rot}} \tag{2.38}$$

with $n = 1, 2$. The important result of these studies [36, 37] is that for strong quadrupole coupling the fastest possible spinning speed is recommended.

The Hartmann-Hahn condition [23] for CP from ^{1}H to low-sensitivity spin-1/2-nuclei can be adjusted using standard compounds, e. g. adamantane and Q_8M_8 for ^{13}C and ^{29}Si[^{1}H] CP MAS NMR, respectively. Similar standard compounds are not conventional for quadrupolar nuclei. Eq. (2.38) allows a basic setting for the mixing pulse. Then, a linear ramp pulse from 84% to 100% (1.5 dB) and a variation of the proton channel transmitter attenuation in 1-dB steps can be used for exact adjustment.

The excitation problem for broad signals will be discussed in Section 2.11. The same problem exists for cross polarization, if it involves signals that cannot be excited by a single monochrome pulse. Harris *et al.* [38] introduced the BRAIN-CP experiment (broadband adiabatic inversion CP), which makes use of the broad, uniformly large frequency profiles of chirped inversion pulses, in order to overcome this problem for spin-1/2 nuclei. The adiabatic process will be discussed in Section 2.10. The extension of the BRAIN-CP method to MAS experiments with half-integer quadrupolar nuclei was described by Wi *et al.* [39, 40].

A review of CP correlation experiments involving half-integer quadrupolar nuclei was published by Deschamps and Massiot [41]. MQMAS experiments with CP between quadrupolar and spin ½ nuclei in both directions were reviewed by Amoureux and Pruski [42]. The number of studies concerning CP between two different quadrupolar nuclei is rather limited. Examples are the investigations of aluminoborate glasses by Chan *et al.* [43] and of corundum (aluminum to oxygen CP) by Haase and Oldfield [44].

Wolf *et al.* [45] adapted the classic static adiabatic demagnetization method of Slichter and Holton [46] for MAS experiments with low radiofrequency nutation fields on both the ^{1}H- and the I-spin channels. The so-called ADRF-CPMAS NMR experiment begins with an adiabatic demagnetization in the rotating frame (ADRF) and can be applied for second-order quadrupole broadened MAS NMR signals.

The classical CP is now in competition with recent magnetization transfer techniques. Giovine *et al.* [47] claimed, "PRESTO (Phase-shifted Recoupling Effects a Smooth Transfer of Order) … is currently the method of choice to achieve the magnetization transfer from protons to quadrupolar nuclei and … has been shown to supersede Cross-Polarization under Magic-Angle Spinning (MAS) for quadrupolar nuclei". A comparison of PRESTO with *D*-RINEPT (Dipolar-mediated Refocused

Insensitive Nuclei Enhanced by Polarization Transfer) gave the result, "PRESTO yields the highest transfer efficiency at low magnetic fields and MAS frequencies, whereas owing to its higher robustness to rf-field inhomogeneity and chemical shifts, *D*-RINEPT is more sensitive at high fields and MAS frequencies" [47]. Another through-space *D*-HMQC (Dipolar Heteronuclear Multiple-Quantum Correlation) experiment [48] was used, in order to correlate the signals of ^{207}Pb isotope with those of neighboring half-integer spin quadrupolar nuclei of ^{11}B in $Pb_4O(BO_3)_2$ crystalline powder. Eliav *et al.* [49] discussed the site-resolved multiple-quantum filtered correlations and distance measurements by MAS NMR and compared the heteronuclear multiple-quantum correlation (HMQC) and heteronuclear single-quantum correlation (HSQC) experiments with rotational-echo double resonance (REDOR), see Section 2.10.

Fast magic angle spinning (MAS) and proton detection is widely used to enhance the sensitivity of solid-state NMR experiments with spin-½-nuclei, but can be applied also to half-integer quadrupolar nuclei. Venkatesh *et al.* [50] showed that "proton detected 2D hetero-nuclear correlation solid-state NMR spectra of half-integer nuclei can still be acquired in about the same time as a 1D spin echo spectrum". Carnahan *et al.* [51] report, "Complete 2D ^{17}O -> ^{1}H *D*-RINEPT correlation NMR spectra were typically obtained in less than 10 h from less than 10 mg of material, with low to moderate O-17 enrichment (less than 20%). Two-dimensional ^{1}H-^{17}O correlation solid-state NMR spectra allow overlapping oxygen sites to be resolved on the basis of proton chemical shifts or by varying the mixing time used for ^{1}H-^{17}O magnetization transfer."

2.9 DNP for Signal Enhancement

Dynamic nuclear polarization (DNP) transfers the relatively high spin polarization of unpaired electrons to coupled nuclear spins using microwave irradiation near the EPR frequency. This sensitivity enhancement technique was proposed in 1953 by Overhauser [52] and verified in 1956 by Carver and Slichter [53] by means of a ^{7}Li double resonance experiment at the NMR frequency of 50 kHz and an EPR frequency of 84 MHz. Developments in instrumentation for cryogenic MAS and high-power microwave sources at extremely high EPR frequencies provided DNP experiments with high-field solid-state NMR. The state-of-art in 2012 was an NMR frequency of 700 MHz and an EPR frequency of 460 GHz [54]. Bruker offers in 2024 DNP-NMR-spectrometers in the range 400—900 MHz (NMR), 263—527 GHz gyrotrons, gain factor 200, measuring temperature about 100 K and MAS frequencies up to 40 kHz.

DNP MAS NMR investigations of half-integer quadrupolar nuclei have increased over the past decade. An example of the enhanced solid-state NMR correlation spectroscopy of ^{27}Al using DNP was presented by Lee *et al.* [55]. DNP-enhanced interface-selective DQ-SQ homonuclear dipolar correlation ^{27}Al MAS NMR spectra were measured at 103 K and showed the correlations of AlO_4, AlO_5 and AlO_6 species in mesoporous alumina [55]. Michaelis *et. al.* [56] demonstrated the dynamic nuclear polarization of ^{17}O nuclei. Blanc *et al.* [57] and Perreras *et al.* [58] reported about natural abundance ^{17}O DNP two-dimensional experiments. Bouleau *et al.* [59] described DNP experiments including quadrupolar nuclei at temperatures down to 30 K and MAS frequencies up to 25 kHz. Kobayashi *et al.* [60] discussed DNP applications with quadrupolar nuclei in heterogeneous catalysis research. Lund *et al.* [61] reported about DNP targeting catalytically active ^{27}Al sites. Valla *et al.* [62] confirmed by DNP that in amorphous aluminosilicates molecular Al and Si precursors are preferentially connected to Al(IV) and Si(IV) interfacial sites, respectively. Brownbill *et al.* [63] studied at 18.8 T the ^{17}O DNP MAS NMR spectrum of ^{17}O enriched $Mg(OH)_2$ and obtained an enhancement factor of 17. Chaudhari *et al.* [64] report an enhancement of over 100 at 18.8 T by means of an enhanced MAS frequency of 40 kHz and studied mesoporous alumina with surface enhanced ^{27}Al cross-polarization. Hope *et al.* [65] demonstrated on CeO_2 nanoparticles a surface-selective enhancement for the first three layers. Perras *et al.* [66] demonstrated that Brønsted acid sites can be directly observed at natural abundance by ^{17}O DNP MAS NMR. Kim *et al.* [67] found by ^{27}Al DNP

MAS NMR spectroscopy how microscopic changes trigger the sudden onset of deactivation of $Ca_3Al_2O_6$-stabilized CaO in the CO_2 uptake process [68]. Mais *et al.* [69] applied ^{27}Al DNP MAS NMR for the characterization of surface sites in γ-alumina. Perras *et al.* [70] have used ^{17}O DNP MAS NMR for the characterization of Zr- and Y-based mesoporous silica-supported single-site catalysts. Wisser *et al.* [71] present a series of new hybrid biradicals for the use in DNP experiments, yields enhancements of up to 185 at 800 MHz ^{1}H frequency and 40 kHz MAS frequency and measure ^{27}Al and ^{29}Si surface enhanced spectra of amorphous aluminosilicates and ^{17}O DNP MAS NMR spectra of silica nanoparticles. Wolf *et al.* [72] demonstrated, " the remarkable efficacy of Mn(II) dopants, used as endogenous polarization agents for MAS-DNP, in enabling the detection of O-17 at a natural abundance of only 0.038%" and found, "Depending on the Mn(II) dopant concentration, we obtain significant signal enhancement factors, 142 and 24, for Li-6 and Li-7 nuclei in LTO, respectively."

Nagashima *et al.* [73] introduced the RINEPT-SR41 2 (tt) sequence. They demonstrated that this ^{1}H → ^{17}O procedure is more efficient than PRESTO or direct DNP for the observation of unprotonated ^{17}O sites. The transfer of DNP-enhanced ^{1}H magnetization to half-integer quadrupolar nuclei in solids at moderate spinning rate was described in a following paper [74]. A so-called DNP-SENS experiment combined D-RINEPT and MQMAS techniques for the investigation of quadrupolar nuclei on the surface of oxide nanoparticles [75].

Articles by Perras *et al.* [76], Leroy and Bryce [77], and Rossini [78], reviewed in 2018 applications of DNP MAS NMR on half-integer quadrupolar nuclei; in 2019 a review was presented by Rankin et al. [79].

2.10 Adiabatic Passage, Excitation by Modulated Pulsing, REDOR

The high-temperature approximation $h\nu_\mathrm{L} \ll kT$ with Boltzmann's constant k applies at least for temperatures above 4 K and Larmor frequencies below 4 GHz. Thus, in NMR spectroscopy spontaneous emission can be neglected. The probabilities for absorption and induced emission are equal and depend on the population p of the two considered energy levels. Using the Boltzmann distribution $\exp(-E_m/kT) \,/\, \sum_m \exp(-E_m/kT)$ in the thermal equilibrium, we can calculate the population ratio for the Zeeman splitting of the $m \to m+1$ transition (see [1] p. 133):

$$\frac{p_{m+1}}{p_m} = \exp\frac{-\hbar\gamma B_0}{kT} = \exp\frac{h\nu_\mathrm{L}}{kT} \approx 1 + \frac{h\nu_\mathrm{L}}{kT}. \tag{2.39}$$

For $(p_{m+1} - p_m)/p_m$ we obtain a relative population difference of $h\nu_\mathrm{L}/kT$; for $\nu_\mathrm{L} = 600\ \mathrm{MHz}$ and $T = 300\ \mathrm{K}$, this amounts to about 1×10^{-4}. As an example, we consider under these conditions a spin-5/2 nucleus with a positive gyromagnetic ratio and apply an arbitrary normalization of $p_{-5/2} = 10\,001$ for the highest energy level $m = -5/2$. Then we have populations of $10\,001, 10\,002, 10\,003, 10\,004, 10\,005,$ and $10\,006$, for $m = -\frac{5}{2}, -\frac{3}{2}, -\frac{1}{2}, \frac{1}{2}, \frac{3}{2}$, and $5/2$, respectively. The excitation of the central transition is based like any single-quantum transition on a population difference one at this scale. But a sequence of adiabatic population inversions, from $-5/2$ to $-3/2$, from $-3/2$ to $-1/2$, from $5/2$ to $3/2$, and finally from $3/2$ to $1/2$, would give a population difference of five and thus a five-fold sensitivity for the central transition.

Adiabatic passages are well known in NMR; see Abragam [1] p. 35. Figure 2.3 shows the way the frequency can be stepped through the region of resonances by changing the offset. This should be done slowly enough that the density operator can follow the Hamiltonian. A criterion for adiabatic inversion is given by the adiabaticity factor [80]:

$$Q(t) = \frac{\gamma B_{\mathrm{eff}}(t)}{\left|\frac{\mathrm{d}\theta(t)}{\mathrm{d}t}\right|} \tag{2.40}$$

with θ as the inclination of B_{eff} with respect to the +x axis in the rotating field. It is recommended that the adiabaticity factor for a linear sweep is greater than or equal to 5 [80]. For WURST or HS pulses an adiabaticity factor of 5 should be applied [2].

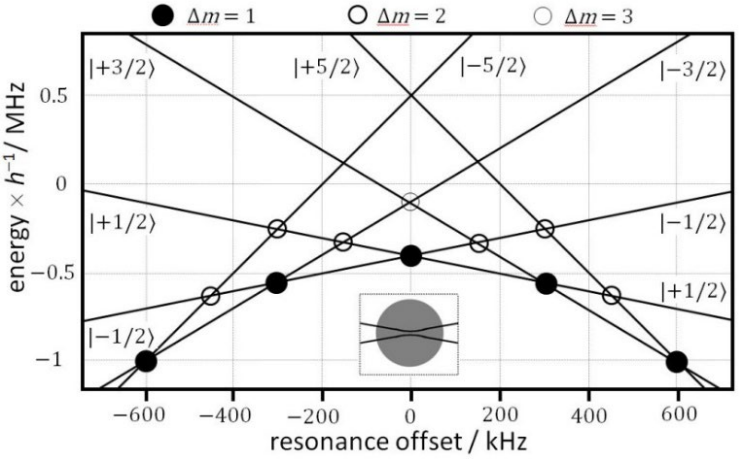

Fig. 2.3. The energy, $E = m\ \Delta\nu\ h$, of the spin states m as a function of the resonance offset, $\Delta\nu$, in the rotating system for an $I = 5/2$, single crystal with the z-axis of EFG coinciding with B_0, no sample rotation, ν_Q = 300 kHz, ν_{RF} = 10 kHz [81]. A crossing of lines as shown in the picture occurs for vanishing RF fields. The RF causes a level repulsion. The circles mark regions of avoided crossings for $\Delta m = 1, 2, 3$. The figure inset shows the level repulsion at the crossing of the −½ and +½ levels with an energy gap of $3h\nu_{RF}$ between the upper and lower branches. The effective RF amplitudes of other level transitions depend on ν_Q as well [81].

We go to Fig. 2.3. Beginning at $m = -5/2$ and switching off the RF power at the Larmor frequency creates a single-quantum coherence like a π/2 pulse applied to a spin-½ system. A full passage from $m = -5/2$ to $m = 5/2$ is comparable with a nonselective π pulse. This means that adiabatic passages can overcome the problem of ill-defined excitation in cases of strong quadrupole interaction. Eigenstate diagrams like Fig. 2.3 for $I = 1$ and $3/2$ were presented by A. J. Vega [32].

The exclusive detection of the $\pm 1/2 \leftrightarrow \pm 3/2$ transitions, based on central-transition signal enhancement by means of an adiabatic RF sweep, was introduced by McDowell *et al.* [82] in order to simplify spectra and increase their intensity. A different approach to intensity enhancement by population transfer between Zeeman levels of the quadrupole spin system with selective pulses and adiabatic frequency sweeps was applied to ^{63}Cu in superconductors by Haase *et al.* [83].

Kentgens [84] established in 1991 the quantitative excitation of a half-integer spin system by a frequency-stepped adiabatic half-passage (FSAHP) on the basis of the approach of Sindorf and Bartuska [85], and introduced in 1999 [86] double-frequency sweeps (DFS) in static, MAS and MQMAS NMR experiments on the basis of an appropriate time-dependent amplitude modulation to the carrier frequency, which was applied earlier by Fu *et al.* [87] to integer spin systems in single crystals. A convergent DFS can be generated by a modulation of the RF, which causes two sidebands that are swept from a start frequency in the region of the outer satellites to reach a final frequency, where the spectral range of the central transition begins. Gains of 1.9 for ^{23}Na and 2.5 for ^{27}Al MAS NMR spectra have been achieved experimentally [88].

The excitation can be also enhanced by the application of fast RF amplitude modulation (FAM), which was introduced by Goldbourt *et al.* [89] for MQMAS; see Section 5.4. DFS uses an easily adjustable frequency modulation, and FAM uses amplitude modulation, which can be performed on spectrometers for which frequency modulation of the short RF pulse is not feasible. There is no difference between DFS and FAM from a physical point of view, since frequency and phase modulations of the RF can give the same result. FAM was improved by Bräuniger *et al.* [90], and a more recent version SW(*tan*)-FAM [91] uses frequency-swept fast-amplitude-modulated pulse trains with a tangent-shaped sweep profile.

NMR transitions can be saturated by irradiation with the corresponding RF frequency. Saturation of a transition yields equal populations of the two involved eigenstates. A hypothetical selective saturation of all satellite transitions in a spin-5/2 system would lead in the example above to populations of 10 002, 10 002, 10 002, 10 005, 10 005, and 10 005, for the levels -5/2, -3/2, -1/2, 1/2, 3/2, and 5/2 , respectively. The population difference for the central transition would increase from one to three. The corresponding increase for spin 3/2 nuclei amounts to two. Yao *et al.* [92] used for the satellite saturation a fast 180°-phase alternating pulse train in MAS experiments and called this approach rotor-assisted population transfer (RAPT). Enhancements of 1.7 and 1.9, near the theoretical value of 2.0, were obtained [92] for ^{23}Na in $Na_2C_2O_4$ and ^{87}Rb in $RbClO_4$ powders, respectively. It should be noted here that the experimentally obtained enhancements for DFS described above are lower than the theoretical values, 5.0 for spin 5/2 and 3.0 for spin 3/2. DFS provides only enhancements of the order which is expected for the saturation of the satellite transitions.

Silver *et al.* [93] found that using as a driving function a complex RF pulse with an envelope of the form of a hyperbolic secant (HS) function of time, while the phase varies as a hyperbolic cosine function, resulted in a population inversion with a very sharply defined bandwidth. The phase modulation yields a hyperbolic tangent function over the frequency range, and the magnetization as a function of the frequency gives a nearly rectangular shape. Siegel *et al.* [94] introduced HS pulses for the signal enhancement of NMR spectra of half-integer quadrupolar nuclei. A comparison between HS and DFS for spin-5/2 nuclei [95] gave almost similar enhancements for static powder and a slightly better value of 3.1 for HS than 2.5 for DFS, normalized by 1.0 for the rectangular pulse without modulation. Nakashima *et al.* [4] explained that it is most useful to choose such an offset that the frequency of the HS pulse is positioned in *one* of the satellites. In a recent review Nakashima and Wasylishen [3] described the sensitivity enhancement by application of HS and other modulated pulses. They conclude [3]: «One simply adjusts the bandwidth of the HS pulse to the MAS frequency and for Spin-3/2 systems, centers the HS pulse near the estimated value of $C_\mathrm{Q}/4$.» This demonstrates an important point regarding the sophisticated methods for enhancing the sensitivity of quadrupolar nuclei: It is useful to know the result before starting the experiment.

Carnevale and Bodenhausen [96] presented a composite pulse consisting of $3 \leq n \leq 7$ rectangular pulses τ_x, $2\ \tau_{-x}$, $3\ \tau_x$, … ,$n\ \tau_{\pm x}$ which caused a time-dependent amplitude modulation where the modulation frequency decreases with time. They denoted it as COMPACT-*n* (composite pulses adapted for central transitions) and obtained a signal enhancement factor of about 1.4 for the central transition [96].

Spin decoupling is widely used in solid-state NMR, and spectra of quadrupolar nuclei also make use of applications of heteronuclear spin decoupling as first shown by A.J. Vega [37]. This is not considered in the present review. Such literature is included in the study of Candran *et al.* [97]. They compared the decoupling efficiency of various multi-pulse decoupling sequences at moderate MAS speeds and found that the frequency-swept decoupling schemes SWf-TPPM and SWf-SPINAL perform significantly better than the conventional TPPM and SPINAL sequences [97]. We note it here, since the frequency-swept decoupling schemes belong to the topic of modulated pulsing.

Another NMR technique that uses adiabatic passage in combination with rotational echo and double resonance was introduced by Gullion [98]. He combined the principles of rotational-echo double resonance (REDOR), with the transfer-of-populations double-resonance (TRAPDOR) developed by Grey *et al.* [99, 100]. The so-called REAPDOR (rotational echo adiabatic passage double resonance) technique allows first, like TRAPDOR, the indirect detection of signals which are too broad to be directly observable for the single-resonance observation of the quadrupole nucleus, and second, like REDOR, the measurement of distances between spin pairs. A first review was written by Gullion and A.J. Vega [101]. Later a similar dipolar recoupling experiment for samples that are not spinning at the magic angle was introduced as SEDOR (spin-echo, double-resonance) [102]. The state-of-art for

distance measurements to quadrupolar nuclei was reviewed in 2021 by Goldbourt [103]. The RESPDOR experiment (rotational echo saturation transfer double resonance) is included [103].

Some additional MQMAS NMR techniques that use adiabatic passage for excitation and conversion will be discussed in Section 5.

2.11 Excitation for Very Broad Signals

The term *broad-line NMR* was used until the seventies as the antonym of *high-resolution NMR*. Since that time the two technically different branches of NMR have converged, and the term *broad-line NMR* in its old meaning disappeared. Broad NMR signals, which can be fully excited by one short pulse, do not require a special broad-line technique. A rectangular π/2 pulse of 1-µs duration has an excitation bandwidth of about 1 MHz (see Eq. (2.07)), but low-gamma nuclei require a longer π/2 pulse with reduced bandwidth. We still need methodologies for the acquisition of very broad signals, for which the name ultra-wideline (UW) NMR spectroscopy was introduced by Tang *et al.* [104, 105]. A review of this field was 2012 written by Schurko [106].

The frequency stepped echo technique requires 30—100 echo measurements with different offsets. The spectrum is presented by the echo amplitude as a function of the offset. The amplitude can be measured directly or determined by the total intensity of its Fourier transformed spectrum. The retuning of the probe after the change offset is an obstacle for automatic measurement.

Massiot *et al.* [107] introduced VOCS (variable-offset cumulative spectrum). They reduced the number of measurements by increasing the spacing between different offsets, Fourier transformed the full-echo FIDs, and added the obtained single spectra to a full powder pattern. Medek *et al.* [108] showed that by means of spin-echo sequences with short and very weak RF pulses, most of the crystallites within the bandwidth of interest can be excited, which enables the acquisition of ideal-like static line shapes even for megahertz-wide central transition patterns.

The quadrupole version QCPMG of the Carr-Purcell Meiboom-Gill pulse sequence [109, 110] will be discussed in Section 3.8. Some studies combine VOCS and QCPMG [111]; see also [106]. The transmitter offset increment has to be a multiple of the Carr-Purcell spikelet distances. O'Dell and Schurko [112] applied a combination of QCPMG and WURST and measured a 500-kHz broad uniform excited ^{71}Ga NMR spectrum of gallium phthalocyanine chloride. O'Dell *et al.* [113] obtained, by a VOCS-style frequency stepped WURST QCPMG pulse sequence, a 3-MHz broad ^{65}Cu spectrum of $(PPh_3)_2CuO_2CCH_3$. Jaroszewicz *et al.* [114] presented a relaxation-assisted separation of overlapping patterns in the broad-line spectra. Wang *et al.* [115] introduced the quadrupole frequency sweep (QFS) as the sum of two DFS and the quadruple WURST (QWURST) as the sum of four WURST for the manipulation of satellite-transition (ST) populations. The inequivalence between field and frequency stepping in external fields up to 36 T was demonstrated in a paper by Hung *et al*. [116]. Jaroszewicz *et al.* [117] introduced for the processing an automated multi-order phase correction routine, in order to overcome the complex frequency-dependent phase dispersions in ultra-wideline NMR spectra.

2.12 References

[1] A. Abragam, Principles of Nuclear Magnetism (paperback reprint 1989), Oxford University Press, Oxford, 1961, pp. 599.

[2] E. Kupce, R. Freeman, Adiabatic Pulses for Wideband Inversion and Broadband Decoupling, J. Magn. Reson. A 115 (1995) 273-276. https://doi.org/10.1006/jmra.1995.1179.

[3] T.T. Nakashima, R.E. Wasylishen, Sensitivity and Resolution Enhancement of Half- integer Quadrupolar Nuclei in Solid-state NMR, in: R.E. Wasylishen, S.E. Ashbrook, S. Wimperis (Eds.), NMR of Quadrupolar Nuclei in Solid Materials, Wiley, Chichester, 2012, pp. 95-106.

[4] T.T. Nakashima, R. Teymoori, R.E. Wasylishen, Using Hyperbolic Secant Pulses to Assist Characterization of Chemical Shift Tensors for Half-integer Spin Quadrupolar Nuclei in MAS Powder Samples, Magn. Reson. Chem. 47 (2009) 465-471. https://doi.org/10.1002/mrc.2413.

[5] M. Garwood, L. DelaBarre, The Return of the Frequency Sweep: Designing Adiabatic Pulses for Contemporary NMR, J. Magn. Reson. 153 (2001) 155-177. https://doi.org/10.1006/jmre.2001.2340.

[6] R. Bhattacharyya, L. Frydman, Quadrupolar NMR Spectroscopy in Solids Using Frequency-swept Echoing Pulses, J. Chem. Phys. 127, 194503 (2007) 1-8. https://doi.org/10.1063/1.2793783.

[7] L.A. O'Dell, The WURST Kind of Pulses in Solid-State NMR, Solid State Nucl. Magn. Reson. 55-56 (2013) 28-41. https://doi.org/https://doi.org/10.1016/j.ssnmr.2013.10.003.

[8] P.A.M. Dirac, The Principles of Quantum Mechanics, Clarendon Press, Oxford, 1958.

[9] D. Fenzke, D. Freude, T. Fröhlich, J. Haase, NMR Intensity Measurements of Half-integer Quadrupole Nuclei, Chem. Phys. Lett. 111 (1984) 171-175. https://doi.org/10.1016/0009-2614(84)80458-3.

[10] P.P. Man, Investigation of the Central Line of ^{55}Mn in $KMnO_4$ by a Two-dimensional NMR Method, J. Magn. Reson. 67 (1986) 78-90. https://doi.org/10.1016/0022-2364(86)90411-7.

[11] N.C. Nielsen, H. Bildsoe, H.J. Jakobsen, Multiple-quantum MAS Nutation NMR Spectroscopy of Quadrupolar Nuclei, J. Magn. Reson. 97 (1992) 149-161. https://doi.org/10.1016/0022-2364(92)90243-Z.

[12] D. Freude, J. Haase, Quadrupole Effects in Solid-State NMR, NMR Basic Principles and Progress 29 (1993) 1-90. https://doi.org/10.1007/978-3-642-50046-6_1.

[13] H.C. Torrey, Transient Nutations in Nuclear Magnetic Resonance, Phys. Rev. 76 (1949) 1059-1068. https://doi.org/10.1103/PhysRev.76.1059.

[14] A. Samoson, E. Lippmaa, Central Transition NMR Excitation Spectra of Half-integer Quadrupole Nuclei, Chem. Phys. Lett. 100 (1983) 205-208. https://doi.org/10.1016/0009-2614(83)87276-5.

[15] A. Samoson, E. Lippmaa, Excitation Phenomena and Line Intensities in High-resolution NMR Spectra of Half-integer Quadrupolar Nuclei, Phys. Rev. B 28 (1983) 6567-6570. https://doi.org/10.1103/PhysRevB.28.6567.

[16] W.S. Veeman, Quadrupole Nutation NMR in Solids, Z. Naturforsch. A 47 (1992) 353-360. https://doi.org/10.1515/zna-1992-1-260.

[17] A.P.M. Kentgens, Off-resonance Nutation NMR Spectroscopy of Half-integer Quadrupolar Nuclei, Progr. Nucl. Magn. Reson. Spectr. 32 (1998) 141-164. https://doi.org/10.1016/S0079-6565(98)00015-6.

[18] A.P.M. Kentgens, Quadrupolar Nutation Spectroscopy, in: R.E. Wasylishen, S.E. Ashbrook, S. Wimperis (Eds.), NMR of Quadrupolar Nuclei in Solid Materials, Wiley, Chichester, 2012, pp. 107-120.

[19] O. Glotova, N. Ponamareva, N. Sinyavsky, B. Nogaj, Non-cyclic Geometric Phase of Nuclear Quadrupole Resonance Signals of Powdered Samples, Solid State Nucl. Magn. Reson. 39 (2011) 1-6. https://doi.org/10.1016/j.ssnmr.2011.02.002.

[20] E.S. Blaakmeer, W.M.J. Franssen, A.P.M. Kentgens, Quadrupolar Nutation NMR to Discriminate Central and Satellite Transitions: Spectral Assignments for a Ziegler-Natta Catalyst, J. Magn. Reson. 281 (2017) 199-208. https://doi.org/10.1016/j.jmr.2017.06.002.

[21] W.M.J. Franssen, E.S. Blaakmeer, A.P.M. Kentgens, Satellite Nutation of Half Integer Quadrupolar Nuclei: Theory and Practice, J. Magn. Reson. 300 (2019) 41-50. https://doi.org/10.1016/j.jmr.2019.01.010.

[22] J. Haase, D. Freude, H. Pfeifer, E. Lippmaa, P. Sarv, Two-Pulse Free Induction Decay Quadrupole NMR, Chem. Phys. Lett. 152 (1988) 254-257. https://doi.org/10.1016/0009-2614(88)87363-9.

[23] J. Haase, H. Pfeifer, A New Two-pulse Free Induction Decay Method to Measure Solid-state NMR Spectra of Quadrupolar Nuclei with Half-integer Spin, J. Magn. Reson. 86 (1990) 217-226. https://doi.org/10.1016/0022-2364(90)90254-7.

[24] P.P. Man, Measurement of Quadrupolar Coupling Constant with a Two-pulse Sequence in Solid-state NMR, Mol. Phys. 69 (1990) 337-346. https://doi.org/10.1080/00268979000100231.

[25] P.P. Man, Determination of the Quadrupolar Coupling Constant in Powdered Samples with a Two In-phase RF Pulse Sequence in Solid-state NMR, Chem. Phys. Lett. 168 (1990) 227-232. https://doi.org/10.1016/0009-2614(90)85134-X.

[26] P.P. Man, Measurement of the Quadrupolar Coupling with Two Pulses of Opposite Phase, J. Magn. Reson. 94 (1991) 258-267. https://doi.org/10.1016/0022-2364(91)90105-3

[27] S.Z. Ageev, P.P. Man, J. Fraissard, B.C. Sanctuary, Determination of Quadrupolar Spin Coupling for Spin 7/2 Using Two Pulse Sequences, Mol. Phys. 91 (1997) 75-80. https://doi.org/10.1080/002689797171751.

[28] S.R. Hartmann, E.L. Hahn, Nuclear Double Resonance in the Rotating Frame, Phys. Rev. 128 (1962) 2042-2053. https://doi.org/10.1103/PhysRev.128.2042.

[29] A. Pines, M.G. Gibby, J.S. Waugh, Proton-enhanced NMR of Dilute Spins in Solids, J. Chem. Phys. 59 (1973) 569-590. https://doi.org/10.1063/1.1680061.

[30] C.P. Slichter, Principles of Magnetic Resonance, Springer Verlag, Berlin, Heidelberg, New York, London, Paris, Tokyo, Hong Kong, 1990.

[31] S. Vega, Multiple-quantum Cross-polarization NMR on Spin Systems with *I*=1/2 and *S*=3/2 in Solids, Phys. Rev. A 23 (1981) 3152-3173. https://doi.org/10.1103/PhysRevA.23.3152.

[32] A.J. Vega, Quadrupolar Nuclei in Solids, in: R.E. Wasylishen, S.E. Ashbrook, S. Wimperis (Eds.), NMR of Quadrupolar Nuclei in Solid Materials, Wiley, Chichester, 2012, pp. 17-44.

[33] C.S. Blackwell, R.L. Patton, Aluminum-27 and Phosphorus-31 NMR Studies of Aluminophosphate Molecular Sieves, J. Phys. Chem. 88 (1984) 6135-6139. https://doi.org/10.1021/j150669a016.

[34] C.A. Fyfe, H. Grondey, K.T. Mueller, K.C. Wongmoon, T. Markus, Coherence Transfer Involving Qadrupolar Nuclei in Solids: 27Al-31P Cross-Polarization NMR in the Molecular Sieve VPI-5, J. Am. Chem. Soc. 114 (1992) 5876-5878. https://doi.org/10.1021/ja00040a069.

[35] M. Pruski, D.P. Lang, C. Fernandez, J.P. Amoureux, Multiple-quantum Magic-angle Spinning NMR with Cross-polarization: Spectral Editing of High-resolution Spectra of Quadrupolar Nuclei, Solid State Nucl. Magn. Reson. 7 (1997) 327-331. https://doi.org/10.1016/S0926-2040(96)01284-2.

[36] A.J. Vega, CP/MAS of Quadrupolar *S*=3/2 Nuclei, Solid State Nucl. Magn. Reson. 1 (1992) 17-32. https://doi.org/10.1016/0926-2040(92)90006-U.

[37] A.J. Vega, MAS NMR Spin Locking of Half-integer Quadrupolar Nuclei, J. Magn. Reson. 96 (1992) 50-68. https://doi.org/0.1016/0022-2364(92)90287-H.

[38] K.J. Harris, A. Lupulescu, B.E.G. Lucier, L. Frydman, R.W. Schurko, Broadband Adiabatic Inversion Pulses for Cross-polarization in Wideline Solid-state NMR Spectroscopy, J. Magn. Reson. 224 (2012) 38-47. https://doi.org/10.1016/j.jmr.2012.08.015.

[39] S. Wi, C. Kim, R. Schurko, L. Frydman, Adiabatic Sweep Cross-Polarization Magic-Angle-Spinning NMR of Half-Integer Quadrupolar Spins, J. Magn. Reson. 277 (2017) 131-142. https://doi.org/10.1016/j.jmr.2017.02.021.

[40] S. Wi, R.W. Schurko, L. Frydman, Broadband Adiabatic Inversion Cross-Polarization Phenomena in the NMR of Rotating Solids, Solid State Nucl. Magn. Reson. 94 (2018) 31-53. https://doi.org/https://doi.org/10.1016/j.ssnmr.2018.08.003.

[41] M. Deschamps, D. Massiot, Correlation Experiments Involving Half-integer Quadrupolar Nuclei, in: R.E. Wasylishen, S.E. Ashbrook, S. Wimperis (Eds.), NMR of Quadrupolar Nuclei in Solid Materials, Wiley, Chichester, 2012, pp. 179-198.

[42] J.-P. Amoureux, M. Pruski, MQMAS NMR: Experimental Strategies, in: R.E. Wasylishen, S.E. Ashbrook, S. Wimperis (Eds.), NMR of Quadrupolar Nuclei in Solid Materials, Wiley, Chichester, 2012, pp. 143-162.

[43] J.C.C. Chan, M. Bertmer, H. Eckert, Site Connectivities in Amorphous Materials Studied by Double-resonance NMR of Quadrupolar Nuclei: High-resolution ^{11}B <-> ^{27}Al Spectroscopy of Aluminoborate Glasses, J. Am. Chem. Soc. 121 (1999) 5238-5248. https://doi.org/10.1021/ja983385i.

[44] J. Haase, E. Oldfield, Aluminum to Oxygen Cross-polarization in α-Al_2O_3 (Corundum), Solid State Nucl. Magn. Reson. 3 (1994) 171-175. https://doi.org/10.1016/0926-2040(94)90012-4.

[45] T. Wolf, S. Jayanthi, A. Lupulescu, L. Frydman, Cross polarization from dipolar-order under magic angle spinning: The ADRF-CPMAS NMR experiment, J. Chem. Phys. 159 (2023) 224304. https://doi.org/10.1063/5.0174955.

[46] C.P. Slichter, W.C. Holton, Adiabatic Demagnetization in a Rotating Reference System, Phys. Rev. 122 (1961) 1701-1708. https://doi.org/10.1103/PhysRev.122.1701.

[47] R. Giovine, J. Trebosc, F. Pourpoint, O. Lafon, J.P. Amoureux, Magnetization Transfer from Protons to Quadrupolar Nuclei in Solid-State NMR Using PRESTO or Dipolar-Mediated Refocused INEPT Methods, J. Magn. Reson. 299 (2019) 109-123. https://doi.org/10.1016/j.jmr.2018.12.016.

[48] H. Nagashima, A.S.L. Thankamony, J. Trebosc, L. Montagne, G. Kerven, J.P. Amoureux, O. Lafon, Observation of Proximities between Spin-1/2 and Quadrupolar Nuclei in Solids: Improved Robustness to Chemical Shielding Using Adiabatic Symmetry-Based Recoupling, Solid State Nucl. Magn. Reson. 94 (2018) 7-19. https://doi.org/10.1016/j.ssnmr.2018.07.001.

[49] U. Eliav, A. Haimovich, A. Goldbourt, Site-Resolved Multiple-Quantum Filtered Correlations and Distance Measurements by Magic-Angle Spinning NMR: Theory and Applications to Spins with Weak to Vanishing Quadrupolar Couplings, J. Chem. Phys. 144 (2016). https://doi.org/10.1063/1.4938415.

[50] A. Venkatesh, M.P. Hanrahan, A.J. Rossini, Proton Detection of MAS Solid-State NMR Spectra of Half-Integer Quadrupolar Nuclei, Solid State Nucl. Magn. Reson. 84 (2017) 171-181. https://doi.org/10.1016/j.ssnmr.2017.03.005.

[51] S.L. Carnahan, B.J. Lampkin, P. Naik, M.P. Hanrahan, Slowing, II, B. VanVeller, G. Wu, A.J. Rossini, Probing O-H Bonding through Proton Detected H-1-O-17 Double Resonance Solid-State NMR Spectroscopy, J. Am. Chem. Soc. 141 (2019) 441-450. https://doi.org/10.1021/jacs.8b10878.

[52] A.W. Overhauser, Polarization of Nuclei in Metals, Phys. Rev. 92 (1953) 411-415. https://doi.org/10.1103/PhysRev.92.411.

[53] T.R. Carver, C.P. Slichter, Experimental Verification of the Overhauser Nuclear Polarization Effect, Phys. Rev. 102 (1956) 975-980. https://doi.org/10.1103/PhysRev.102.975.

[54] A.B. Barnes, E. Markhasin, E. Daviso, V.K. Michaelis, E.A. Nanni, S.K. Jawla, E.L. Mena, R. DeRocher, A. Thakkar, P.P. Woskov, J. Herzfeld, R.J. Temkin, R.G. Griffin, Dynamic Nuclear Polarization at 700MHz/460GHz, J. Magn. Reson. 224 (2012) 1-7. https://doi.org/https://doi.org/10.1016/j.jmr.2012.08.002.

[55] D. Lee, H. Takahashi, A.S.L. Thankamony, J.P. Dacquin, M. Bardet, O. Lafon, G. De Paepe, Enhanced Solid-State NMR Correlation Spectroscopy of Quadrupolar Nuclei Using Dynamic Nuclear Polarization, J. Am. Chem. Soc. 134 (2012) 18491-18494. https://doi.org/10.1021/ja307755t.

[56] V.K. Michaelis, B. Corzilius, A.A. Smith, R.G. Griffin, Dynamic Nuclear Polarization of ^{17}O: Direct Polarization, J. Phys. Chem. B 117 (2013) 14894-14906. https://doi.org/10.1021/jp408440z.

[57] F. Blanc, L. Sperrin, D.A. Jefferson, S. Pawsey, M. Rosay, C.P. Grey, Dynamic Nuclear Polarization Enhanced Natural Abundance ^{17}O Spectroscopy, J. Am. Chem. Soc. 135 (2013) 2975-2978. https://doi.org/10.1021/ja4004377.

[58] F.A. Perras, T. Kobayashi, M. Pruski, Natural Abundance ^{17}O DNP Two-Dimensional and Surface-Enhanced NMR Spectroscopy, J. Am. Chem. Soc. 137 (2015) 8336-8339. https://doi.org/10.1021/jacs.5b03905.

[59] E. Bouleau, P. Saint-Bonnet, F. Mentink-Vigier, H. Takahashi, J.F. Jacquot, M. Bardet, F. Aussenac, A. Purea, F. Engelke, S. Hediger, D. Lee, G. De Paepe, Pushing NMR Sensitivity Limits Using Dynamic Nuclear Polarization with Closed-loop Cryogenic Helium Sample Spinning, Chem. Sci. 6 (2015) 6806-6812. https://doi.org/10.1039/c5sc02819a.

[60] T. Kobayashi, F.A. Perras, Slowing, II, A.D. Sadow, M. Pruski, Dynamic Nuclear Polarization Solid-State NMR in Heterogeneous Catalysis Research, ACS Catal. 5 (2015) 7055-7062. https://doi.org/10.1021/acscatal.5b02039.

[61] A. Lund, M.F. Hsieh, T.A. Siaw, S.I. Han, Direct Dynamic Nuclear Polarization Targeting Catalytically Active ^{27}Al Sites, Phys. Chem. Chem. Phys. 17 (2015) 25449-25454. https://doi.org/10.1039/c5cp03396a.

[62] M. Valla, A.J. Rossini, M. Caillot, C. Chizallet, P. Raybaud, M. Digne, A. Chaumonnot, A. Lesage, L. Emsley, J.A. van Bokhoven, C. Coperet, Atomic Description of the Interface between Silica and Alumina in Aluminosilicates through Dynamic Nuclear Polarization Surface-Enhanced NMR Spectroscopy and First-Principles Calculations, J. Am. Chem. Soc. 137 (2015) 10710-10719. https://doi.org/10.1021/jacs.5b06134.

[63] N.J. Brownbill, D. Gajan, A. Lesage, L. Emsley, F. Blanc, Oxygen-17 Dynamic Nuclear Polarisation Enhanced Solid-State NMR Spectroscopy at 18.8 T, Chem. Commun. 53 (2017) 2563-2566. https://doi.org/10.1039/c6cc09743j.

[64] S.R. Chaudhari, D. Wisser, A.C. Pinon, P. Berruyer, D. Gajan, P. Tordo, O. Ouari, C. Reiter, F. Engelke, C. Coperet, M. Lelli, A. Lesage, L. Emsley, Dynamic Nuclear Polarization Efficiency Increased by Very Fast Magic Angle Spinning, J. Am. Chem. Soc. 139 (2017) 10609-10612. https://doi.org/10.1021/jacs.7b05194.

[65] M.A. Hope, D.M. Halat, P. Magusin, S. Paul, L.M. Peng, C.P. Grey, Surface-Selective Direct ^{17}O DNP NMR of CeO_2 Nanoparticles, Chem. Comm. 53 (2017) 2142-2145. https://doi.org/10.1039/c6cc10145c.

[66] F.A. Perras, Z.R. Wang, P. Naik, Slowing, II, M. Pruski, Natural Abundance ^{17}O DNP NMR Provides Precise O-H Distances and Insights into the Bronsted Acidity of Heterogeneous Catalysts, Angew. Chem. Int. Ed. 56 (2017) 9165-9169. https://doi.org/10.1002/anie.201704032.

[67] S.M. Kim, W.C. Liao, A.M. Kierzkowska, T. Margossian, D. Hosseini, S. Yoon, M. Broda, C. Coperet, C.R. Muller, In Situ XRD and Dynamic Nuclear Polarization Surface Enhanced NMR Spectroscopy Unravel the Deactivation Mechanism of CaO-Based, $Ca_3Al_2O_6$-Stabilized CO_2 Sorbents, Chem. Mater. 30 (2018) 1344-1352. https://doi.org/10.1021/acs.chemmater.7b05034.

[68] W.Z. Li, Q. Wang, J. Xu, F. Aussenac, G.D. Qi, X.L. Zhao, P. Gao, C. Wang, F. Deng, Probing the Surface of γ-Al_2O_3 by Oxygen-17 Dynamic Nuclear Polarization Enhanced Solid-State NMR Spectroscopy, Phys. Chem. Chem. Phys. 20 (2018) 17218-17225. https://doi.org/10.1039/c8cp03132k.

[69] M. Mais, S. Paul, N.S. Barrow, J.J. Titman, Dynamic Nuclear Polarisation Enhanced Solid-State Nuclear Magnetic Resonance Studies of Surface Modification of γ-Alumina, Johnson Matthey Tech. 62 (2018) 271-278. https://doi.org/10.1595/205651318x696765.

[70] F.A. Perras, K.C. Boteju, Slowing, II, A.D. Sadow, M. Pruski, Direct O-17 Dynamic Nuclear Polarization of Single-Site Heterogeneous Catalysts, Chem. Comm. 54 (2018) 3472-3475. https://doi.org/10.1039/c8cc00293b.

[71] D. Wisser, G. Karthikeyan, A. Lund, G. Casano, H. Karoui, M. Yulikov, G. Menzildjian, A.C. Pinon, A. Purea, F. Engelke, S.R. Chaudhari, D. Kubicki, A.J. Rossini, I.B. Moroz, D. Gajan, C. Coperet, G. Jeschke, M. Lelli, L. Emsley, A. Lesage, O. Ouari, BDPA-Nitroxide Biradicals Tailored for Efficient Dynamic Nuclear Polarization Enhanced Solid-State NMR at Magnetic Fields up to 21.1 T, J. Am. Chem. Soc. 140 (2018) 13340-13349. https://doi.org/10.1021/jacs.8b08081.

[72] T. Wolf, S. Kumar, H. Singh, T. Chakrabarty, F. Aussenac, A.I. Frenkel, D.T. Major, M. Leskes, Endogenous Dynamic Nuclear Polarization for Natural Abundance O-17 and Lithium NMR in the Bulk of Inorganic Solids, J. Am. Chem. Soc. 141 (2019) 451-462. https://doi.org/10.1021/jacs.8b11015.

[73] H. Nagashima, J. Trébosc, Y. Kon, K. Sato, O. Lafon, J.P. Amoureux, Observation of Low-γ Quadrupolar Nuclei by Surface-Enhanced NMR Spectroscopy, J. Am. Chem. Soc. 142 (2020) 10659-10672. https://doi.org/10.1021/jacs.9b13838.

[74] H. Nagashima, J. Trébosc, Y. Kon, O. Lafon, J.P. Amoureux, Efficient transfer of DNP-enhanced ^{1}H magnetization to half-integer quadrupolar nuclei in solids at moderate spinning rate, Magn. Reson. Chem. 59 (2021) 920-939. https://doi.org/10.1002/mrc.5121.

[75] H. Nagashima, F. Maleki, J. Trebosc, R. Belgamwar, V. Polshettiwar, M. Kahn, Y. Kon, G. Pacchioni, O. Lafon, J.P. Amoureux, Probing the Surface of Oxide Nanoparticles Using DNP-Enhanced High-Resolution NMR of Quadrupolar Nuclei, J. Phys. Chem. Lett. 15 (2024) 4858-4863. https://doi.org/10.1021/acs.jpclett.4c00563.

[76] F.A. Perras, T. Kobayashi, M. Pruski, Growing Signals from the Noise: Challenging Nuclei in Materials DNP, eMagRes 7 (2018) 35-50. https://doi.org/10.1002/9780470034590.emrstm1556.

[77] C. Leroy, D.L. Bryce, Recent Advances in Solid-State Nuclear Magnetic Resonance Spectroscopy of Exotic Nuclei, Progr. Nucl. Magn. Reson. Spectr. 109 (2018) 160-199. https://doi.org/10.1016/j.pnmrs.2018.08.002.

[78] A.J. Rossini, Materials Characterization by Dynamic Nuclear Polarization-Enhanced Solid-State NMR Spectroscopy, J. Phys. Chem. Lett. 9 (2018) 5150-5159. https://doi.org/10.1021/acs.jpclett.8b01891.

[79] A.G.M. Rankin, J. Trébosc, F. Pourpoint, J.P. Amoureux, O. Lafon, Recent Developments in MAS DNP-NMR of Materials, Solid State Nucl. Magn. Reson. 101 (2019) 116-143. https://doi.org/10.1016/j.ssnmr.2019.05.009.

[80] J. Baum, R. Tycko, A. Pines, Broadband and Adiabatic Inversion of a Two-level System by Phase-modulated Pulses, Phys. Rev. A 32 (1985) 3435-3447. https://doi.org/10.1103/PhysRevA.32.3435.

[81] J. Haase, M.S. Conradi, C.P. Grey, A.J. Vega, Population Transfers for NMR of Quadrupolar Spins in Solids, J. Magn. Reson. A 109 (1994) 90-97. https://doi.org/10.1006/jmra.1994.1138.

[82] A.F. McDowell, M.S. Conradi, J. Haase, First-satellite Spectroscopy, a New Method for Quadrupolar Spins, J. Magn. Reson. A 119 (1996) 211-218. https://doi.org/10.1006/jmra.1996.0075.

[83] J. Haase, N.J. Curro, R. Stern, C.P. Slichter, New Double Resonance Technique for Quadrupolar Nuclei, Molec. Phys. 95 (1998) 891-896. https://doi.org/10.1080/002689798166512.

[84] A.P.M. Kentgens, Quantitative Excitation of Half-integer Quadrupolar Nuclei by a Frequency-stepped Adiabatic Half-passage, J. Magn. Reson. 95 (1991) 619-625. https://doi.org/10.1016/0022-2364(91)90179-W.

[85] D.W. Sindorf, V.J. Bartuska, Wide-line NMR Spectroscopy in Solids Using Variable Frequency Pulses, J. Magn. Reson. 85 (1989) 581-585. https://doi.org/10.1016/0022-2364(89)90248-5.

[86] A.P.M. Kentgens, R. Verhagen, Advantages of Double Frequency Sweeps in Static, MAS and MQMAS NMR of Spin *I* = 3/2 Nuclei, Chem. Phys. Lett. 300 (1999) 435-443. https://doi.org/0.1016/S0009-2614(98)01402-X.

[87] R.Q. Fu, V.L. Ermakov, G. Bodenhausen, Divergent Double Chirp Pulses for Refocusing Quadrupolar Interactions, Solid State Nucl. Magn. Reson. 7 (1996) 1-10. https://doi.org/10.1016/0926-2040(96)01231-3.

[88] D. Iuga, A.P.M. Kentgens, Influencing the Satellite Transitions of Half-integer Quadrupolar Nuclei for the Enhancement of Magic Angle Spinning Spectra, J. Magn. Reson. 158 (2002) 65-72. https://doi.org/10.1016/S1090-7807(02)00061-7.

[89] A. Goldbourt, P.K. Madhu, Multiple-quantum Magic-angle Spinning: High-resolution Solid-state NMR of Half-integer Spin Quadrupolar Nuclei, Annu. Rep. Nucl. Magn. Reson. Spectrosc. 54 (2005) 81-153. https://doi.org/10.1016/S0066-4103(04)54003-6.

[90] T. Bräuniger, G. Hempel, P.K. Madhu, Fast Amplitude-modulated Pulse Trains with Frequency Sweep (SW-FAM) in Static NMR of Half-integer Spin Quadrupolar Nuclei, J. Magn. Reson. 181 (2006) 68-78. https://doi.org/10.1016/j.jmr.2006.03.016.

[91] T. Bräuniger, Enhancing the Central-transition NMR Signal of Quadrupolar Nuclei by Spin Population Transfer Using SW-FAM Pulse Trains with a Tangent-Shaped Sweep Profile, Solid State Nucl. Magn. Reson. 45-46 (2012) 16-22. https://doi.org/10.1016/j.ssnmr.2012.04.002.

[92] Z. Yao, H.T. Kwak, D. Sakellariou, L. Emsley, P.J. Grandinetti, Sensitivity Enhancement of the Central Transition NMR Signal of Quadrupolar Nuclei under Magic-angle Spinning, Chem. Phys. Lett. 327 (2000) 85-90. https://doi.org/10.1016/S0009-2614(00)00805-8.

[93] M.S. Silver, R.I. Joseph, C.N. Chen, V.J. Sank, D.I. Hoult, Selective Population Inversion in NMR, Nature 310 (1984) 681-683. https://doi.org/10.1038/310681a0.

[94] R. Siegel, T.T. Nakashima, R.E. Wasylishen, Sensitivity enhancement of NMR spectra of half-integer spin quadrupolar nuclei in solids using hyperbolic secant pulses, J. Magn. Reson. 184 (2007) 85-100. https://doi.org/10.1016/j.jmr.2006.09.007.

[95] R. Siegel, T.T. Nakashima, R.E. Wasylishen, Sensitivity Enhancement of Solid-state NMR Spectra of Half-integer Spin Quadrupolar Nuclei Using Hyperbolic Secant Pulses: Applications to Spin-5/2 Nuclei, Chem. Phys. Lett. 421 (2006) 529-533. https://doi.org/10.1016/j.cplett.2006.01.107.

[96] D. Carnevale, G. Bodenhausen, Composite pulses for efficient excitation of half-integer quadrupolar nuclei in NMR of static and spinning solid samples, Chem. Phys. Lett. 530 (2012) 120-125. https://doi.org/10.1016/j.cplett.2012.01.058.

[97] C.V. Chandran, G. Hempel, T. Bräeuniger, ^{19}F--decoupling of Half-integer Spin Quadrupolar Nuclei in Solid-state NMR: Application of Frequency-swept Decoupling Methods, Solid State Nucl. Magn. Reson. 40 (2011) 84-87. https://doi.org/10.1016/j.ssnmr.2011.07.003.

[98] T. Gullion, Measurement of Dipolar Interactions between Spin-1/2 and Quadrupolar Nuclei by Rotational-echo, Adiabatic-passage, Double-resonance NMR, Chem. Phys. Lett. 246 (1995) 25-330. https://doi.org/10.1016/0009-2614(95)01120-X.

[99] C.P. Grey, A.J. Vega, Determination of the Quadrupole Coupling Constant of the Invisible Aluminum Spins in Zeolite HY with ^{1}H-/^{27}Al TRAPDOR, J. Am. Chem. Soc. 117 (1995) 8232-8242. https://doi.org/10.1021/ja00136a022.

[100] C.P. Grey, W.S. Veeman, A.J. Vega, Rotational Ech ^{14}N/^{13}C/^{1}H Triple Resonance Solid-state NMR - A Probe of ^{13}C-^{14}N Internuclear Distances, J. Chem. Phys. 98 (1993) 7711-7724. https://doi.org/10.1063/1.464579.

[101] T. Gullion, A.J. Vega, Measuring Heteronuclear Dipolar Couplings for I=1/2, S > 1/2 Spin Pairs by REDOR and REAPDOR NMR, Progr. Nucl. Magn. Reson. Spectr. 47 (2005) 123-136. https://doi.org/10.1016/j.pnmrs.2005.08.004.

[102] T. Gullion, Dipolar Recoupling of I=1/2, S=3/2 Spin Pairs with SEDOR for Static and Spinning Samples, Magn. Reson. Chem. 45 (2007) S65-S67. https://doi.org/10.1002/mrc.2083.

[103] A. Goldbourt, Distance measurements to quadrupolar nuclei: Evolution of the rotational echo double resonance technique, Magn. Reson. Chem. 59 (2021) 908-919. https://doi.org/https://doi.org/10.1002/mrc.5150.

[104] J.A. Tang, J.D. Masuda, T.J. Boyle, R.W. Schurko, Ultra-wideline ^{27}Al NMR Investigation of Three- and Five-coordinate Aluminum Environments, Chemphyschem 7 (2006) 117-130. https://doi.org/10.1002/cphc.200500343.

[105] J.A. Tang, L.A. O'Dell, P.M. Aguiar, B.E.G. Lucier, D. Sakellariou, R.W. Schurko, Application of Static Microcoils and WURST Pulses for Solid-state Ultra-wideline NMR Spectroscopy of Quadrupolar Nuclei, Chem. Phys. Lett. 466 (2008) 227-234. https://doi.org/10.1016/j.cplett.2008.10.044.

[106] R.W. Schurko, Acquisition of Wideline Solid-State NMR Spectra of Quadrupolar Nuclei, in: R.E. Wasylishen, S.E. Ashbrook, S. Wimperis (Eds.), NMR of Quadrupolar Nuclei in Solid Materials, Wiley, Chichester, 2012, pp. 77-94.

[107] D. Massiot, I. Farnan, N. Gautier, D. Trumeau, A. Trokiner, J.P. Coutures, ^{71}Ga and ^{69}Ga NMR Study of β-Ga_2O_3: Resolution of Four- and Six-fold Coordinated Ga Sites in Static Conditions, Solid State Nucl. Magn. Reson. 4 (1995) 241-248. https://doi.org/10.1016/0926-2040(95)00002-8.

[108] A. Medek, V. Frydman, L. Frydman, Central Transition NMR in the Presence of Large Quadrupole Couplings: Cobalt-59 NMR of Cobaltophthalocyanines, J. Phys. Chem. A 103 (1999) 4830-4835. https://doi.org/10.1021/jp990410d.

[109] F.H. Larsen, H.J. Jakobsen, P.D. Ellis, N.C. Nielsen, Sensitivity-enhanced Quadrupolar-echo NMR of Half-integer Quadrupolar nuclei. Magnitudes and Relative Orientation of Chemical Shielding and Quadrupolar Coupling Tensors, J. Phys. Chem. A 101 (1997) 8597-8606. https://doi.org/10.1021/jp971547b.

[110] I. Hung, Z.H. Gan, On the Practical Aspects of Recording Wideline QCPMG NMR Spectra, J. Magn. Reson. 204 (2010) 256-265. https://doi.org/10.1016/j.jmr.2010.03.001.

[111] J.M. Griffin, A.J. Berry, S.E. Ashbrook, Observation of "Hidden" Magnesium: First-principles Calculations and Mg-25 Solid-state NMR of Enstatite, Solid State Nucl. Magn. Reson. 40 (2011) 91-99. https://doi.org/10.1016/j.ssnmr.2011.08.004.

[112] L.A. O'Dell, R.W. Schurko, QCPMG Using Adiabatic Pulses for Faster Acquisition of Ultra-wideline NMR Spectra, Chem. Phys. Lett. 464 (2008) 97-102. https://doi.org/10.1016/j.cplett.2008.08.095.

[113] L.A. O'Dell, A.J. Rossini, R.W. Schurko, Acquisition of Ultra-wideline NMR Spectra from Quadrupolar Nuclei by Frequency Stepped WURST-QCPMG, Chem. Phys. Lett. 468 (2009) 330-335. https://doi.org/10.1016/j.cplett.2008.12.044.

[114] M.J. Jaroszewicz, L. Frydman, R.W. Schurko, Relaxation-Assisted Separation of Overlapping Patterns in Ultra-Wideline NMR Spectra, J. Phys. Chem. A 121 (2017) 51-65. https://doi.org/10.1021/acs.jpca.6b10007.

[115] Q. Wang, J. Trebosc, Y.X. Li, O. Lafon, S.H. Xin, J. Xu, B.W. Hu, N.D. Feng, J.P. Amoureux, F. Deng, Uniform Signal Enhancement in MAS NMR of Half-Integer Quadrupolar Nuclei Using Quadruple-Frequency Sweeps, J. Magn. Reson. 293 (2018) 92-103. https://doi.org/10.1016/j.jmr.2018.06.005.

[116] I. Hung, A.R. Altenhof, R.W. Schurko, D.L. Bryce, O.H. Han, Z. Gan, Field-stepped ultra-wideline NMR at up to 36 T: On the inequivalence between field and frequency stepping, Magn. Reson. Chem. 59 (2021) 951-960. https://doi.org/https://doi.org/10.1002/mrc.5128.

[117] M.J. Jaroszewicz, A.R. Altenhof, R.W. Schurko, L. Frydman, An automated multi-order phase correction routine for processing ultra-wideline NMR spectra, J. Magn. Reson. 354 (2023) 107528. https://doi.org/https://doi.org/10.1016/j.jmr.2023.107528.